

**Université Pierre et Marie Curie, École des Mines de Paris  
& École Nationale du Génie Rural des Eaux et des Forêts**

---

**Master 2 Sciences de l'Univers, Environnement, Ecologie**

**Parcours Hydrologie-Hydrogéologie**

**Spatial interpolation of precipitation in the Norte Chico region,  
Chile.**

**Pierre-Yves Bourgin**

**Directeurs de recherche: Vazken Andreassian, Simon Gascoin**



Cemagref, centre d'Antony, unité HBAN  
Parc de Tourvoie, BP 44, F-92163 Antony Cedex



Centro de Estudios Avanzados en Zonas Áridas  
Raul Biltran s/n, La Serena Chile

**Year 2009-2010**



## Acknowledgments

I would like to express my sincere gratitude to my supervisors Dr. Simon Gascoin and Dr. Vazken Andreassian for having encouraged and supported this work. The availability, patience and unlimited support they provided were essential to the achievement of this internship. Above all, they made possible this cooperation between their respective laboratories in France and Chile. A long-term stay in a foreign country is always an unforgettable experience and I am really indebted to them for permitting me to take this opportunity. The scientific cooperation was also fulfilling for each part.

My gratitude goes also to all staff members and researchers of both CEAZA and Cemagref. I will leave with regret the first ones and meet again with great pleasure the second ones. The missions on the field and more generally the good times with all of them were a precious support and a pleasant way to learn from their experience.

For having interfered between my supervisors and making this internship possible, I would like to gratefully thank Dr. Pierre Ribstein, supervisor of the Master of Science Hydrology and Hydrogeology of Paris 6. Through him, all professors of the master receive here my gratitude for this instructive year and the joy they always showed in conveying their passion.

Last but not least, my thoughts go to my future colleagues Didier Richard and Nicolle Mathys from the Cemagref, Grenoble. The internship I accomplished 2 years ago with them was the beginning of the all story.

## Abstract

The Norte Chico (26°S-32°S) is a mountainous dominated and semi-arid region located in northern Chile. This region is characterized by a strong east-west topographic gradient since only 200 km separate the coastline from the Andes. The annual precipitation is generally lower than 100 mm along the coast and exceeds 300 mm in the high mountains, where most precipitation occur as snow in winter. Thus, the water resource primarily relies on the melt of seasonal snowpack accumulated in altitude.

The objective in this study is to assess the spatial distribution of precipitation in the Norte Chico, by focusing on the high-altitude areas and to improve the knowledge of the water balance at the regional scale.

We applied a method of elevation-dependent regionalization developed by Valery [2009] to 75 precipitation gauges. The results were compared to previous studies and different methods of interpolation on three levels of test and validation using precipitation observations, snow depth measurements and remotely sensed data. The method of Valery [2009] gave better results. In particular, the runoff coefficients in high-altitude catchments calculated with this spatial distribution of precipitation are more realistic than those obtained by Favier and al. [2009]. As such, this method is valuable to better represent the high altitude water balance in the Norte Chico and this work may provide a sound basis to further hydrological studies in the region.

## Table of Contents

<b>Acknowledgments</b> .....	<b>2</b>
<b>Abstract</b> .....	<b>3</b>
<b>Table of Contents</b> .....	<b>4</b>
<b>Introduction</b> .....	<b>6</b>
<b>1. Description of the Norte-Chico region</b> .....	<b>7</b>
1.1. Seasonal variability .....	8
1.1. Interannual variability.....	8
1.2. Hydrology in mountainous areas .....	9
<b>2. Presentation of previous studies and methods for estimating the spatial distribution of precipitation</b> .....	<b>10</b>
2.1. Interpolation models based on fields observations .....	10
2.1.1. Basic interpolation models.....	10
2.1.1.1. The Thiessen polygons method .....	10
2.1.1.2. The isohyets method .....	10
2.1.1.3. A simple interpolation scheme .....	11
2.1.2. Geostatistical approaches .....	11
2.1.2.1. Inverse Distance Weighted interpolation method (IDW) .....	11
2.1.2.2. Elevation dependency in geostatistical approaches .....	12
2.2. Consideration of atmospheric prediction model .....	12
<b>3. Description of the data and the orographic correction factor method</b> .....	<b>13</b>
3.1. Data .....	13
3.1.1. Precipitation gauges and runoff stations .....	13
3.1.2. Snowfall measurement and snow water equivalent.....	13
3.1.2.1. Available data .....	14
3.1.3. Remote sensing data .....	16
3.1.3.1. Satellite imagery .....	16
3.1.3.2. The Tropical Rainfall Measuring Mission project (TRMM).....	16
3.1.4. Digital Elevation Model .....	17
3.2. Elevation-dependent regionalization method .....	17
3.2.1. The calibration of the model – Cross-validation by jack-knife procedure .....	18
3.2.2. Efficiency functions .....	18
<b>4. Results</b> .....	<b>20</b>
4.1. Characterization of the model parameters.....	20
4.1.1. Results of optimization.....	20
4.1.2. Attempts to improve the orographic correction factor model .....	21

4.1.2.1.	A spatial distribution of orographic correction factors.....	21
4.1.2.2.	A seasonal distribution of orographic correction factors .....	22
4.1.2.3.	Impact of ENSO .....	22
4.1.2.4.	The weather-dependence.....	23
4.1.2.5.	Conclusions .....	23
<b>4.2.</b>	<b>First level of validation – Cross-validation .....</b>	<b>23</b>
4.2.1.	Discussion of the impacts of the orographic correction factor .....	26
4.2.2.	Spatial distribution of precipitation .....	28
<b>4.3.</b>	<b>Second level of validation: Comparison with other precipitation measurements .....</b>	<b>29</b>
4.3.1.	Monthly TRMM predictions over precipitation gauges .....	29
4.3.2.	Brief qualitative analysis of results from previous studies.....	32
4.3.3.	Determining the period of solid precipitation .....	32
4.3.4.	Comparison between estimations and snow water equivalent measurements.....	32
4.3.4.1.	Daily SWE measurements .....	32
4.3.4.2.	Monthly and variable SWE measurements.....	33
<b>4.4.</b>	<b>Third level of validation: Runoff coefficients and water balance .....</b>	<b>36</b>
4.4.1.	Runoff coefficients .....	36
4.4.1.1.	Simple interpolation scheme [ <i>Favier et al., 2009</i> ] .....	37
4.4.1.2.	Consideration of atmospheric prediction model [ <i>Favier et al., 2009</i> ].....	37
4.4.1.3.	TRMM .....	37
4.4.2.	Water balance calculation.....	38
4.4.2.1.	Method – Simplified water balance.....	38
4.4.2.2.	Water losses from snow cover surface - Estimation of mean sublimation .....	38
<b>5.</b>	<b>Error assessment .....</b>	<b>42</b>
	<b>Conclusions .....</b>	<b>43</b>
	<b>Bibliography.....</b>	<b>44</b>

## Introduction

The mountainous regions all over the world are generally considered as water towers. It is estimated that one billion people relies on the water provided by glaciers and melt of seasonal snow-pack from mountain areas [Barnett *et al.*, 2005]. The knowledge of hydrological processes and above all the precipitation is therefore essential in these regions. Among those, the arid and semiarid regions are particularly in jeopardy since they rely almost exclusively on the seasonal melt of snow packs accumulated in the highest parts of watersheds during the wet season (for instance northwestern India, areas south of the Hindu Kush, Western Interior of the U.S.A, North Africa).

The so-called region of Norte Chico (from 26°S to 32°S) in Chile is an example of such semi-arid region which is largely dependent on snow melt water from the mountains. Moreover the rapid socio-economic development of this region relies on irrigated agriculture, mining and increasing tourism activity, all of three requiring large amounts of fresh water [Souvignet, 2007] [Vicuna *et al.*, 2010a]. In spite of this concern about the water resources, an overall understanding of the hydrological processes in the Andean catchments of the Norte Chico is still lacking [Favier *et al.*, 2009].

Because catchments are mountainous, the access to the study area is difficult and the network of precipitation gauges is therefore loose. Moreover the precipitations in mountain areas are known to be extremely variable, both spatially and temporally [Barry, 2008]. As a consequence, closing the water balance of these mountainous, snow-driven catchments is challenging [Favier *et al.*, 2009] and the hydrologists have to design some new methods to improve their knowledge of precipitation input for further hydrological studies. Favier and al. [2009] faced this problem in the study of Norte Chico region revealing large discrepancies between discharge and precipitation for the high-altitude catchments.

The objective in this study is to find an appropriate method for assessing the spatial distribution of precipitation in the Norte Chico, by focusing on the high-altitude areas. This step is essential in order to improve the knowledge of the water balance at the regional scale.

We apply a method of elevation-dependent regionalization developed by Valery [2009] during her PhD at Cemagref to 75 precipitation gauges. We compare the results with the results of previous studies, remotely sensed data and local snow depth measurements.

This work is organized as follows. After a description of the study region and the previous works, we present the elevation-dependent regionalization method and the data. Then, the results of the interpolation are tested and compared to other methods. Simple hydrological budgets are computed to evaluate the benefits for the water balance closure.

# 1. Description of the Norte-Chico region



Photography 1 – Pascua-Lama (around 4100m a.s.l.)



Photography 2 – Pisco Elqui in Elqui valley (1300m a.s.l.)



Photography 3 – Near Punto Choros in Elqui valley (10m a.s.l.)

The Norte Chico region is located in northern Chile between 26°S and 32°S (Figure 1). This region is characterized by a dramatic east-west topographic gradient. Only 200 km

separate the Pacific Ocean coastline from the Argentinean boarder in the Andes, where the altitude can exceed 5000 m. The consequence is a strong longitudinal climatic gradient. The annual precipitation is generally lower than 100 mm along the coast and exceeds 300 mm in the high mountains. Conversely, the mean annual temperature decreases eastward, in such a way that, at the regional scale, most precipitation falls in the form of snow (Photography 1). On the other hand, the Norte Chico's population and agricultural resources are concentrated in low altitude semi-arid areas (Photography 2 and 3), where river flow is extensively used for irrigation. This means that water input areas are separated from the output areas [Gascoin, 2009].

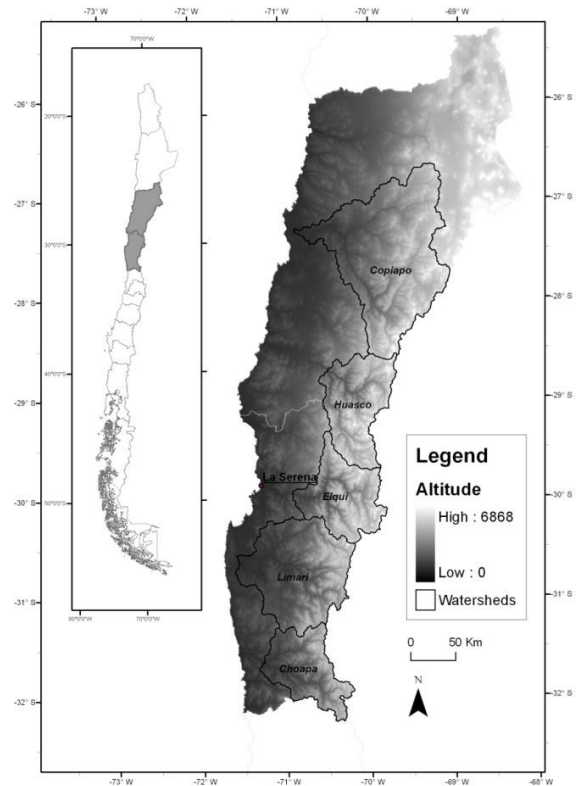


Figure 1 - Location of the region Norte Chico

## 1.1. Seasonal variability

The seasonal cycle of precipitation is very pronounced with a dry season lasting 6 to 12 months (Figure 3). The maximum of precipitation occurs in winter (JJA). Temperature also displays a strong seasonal cycle. The minimum occurs in June-August, coinciding with precipitation maximum and hence snowfall occurs over large areas [Favier *et al.*, 2009] (Figure 2). The time lag between precipitation and discharge characterizes a snow-driven hydrological regime (Figure 3).

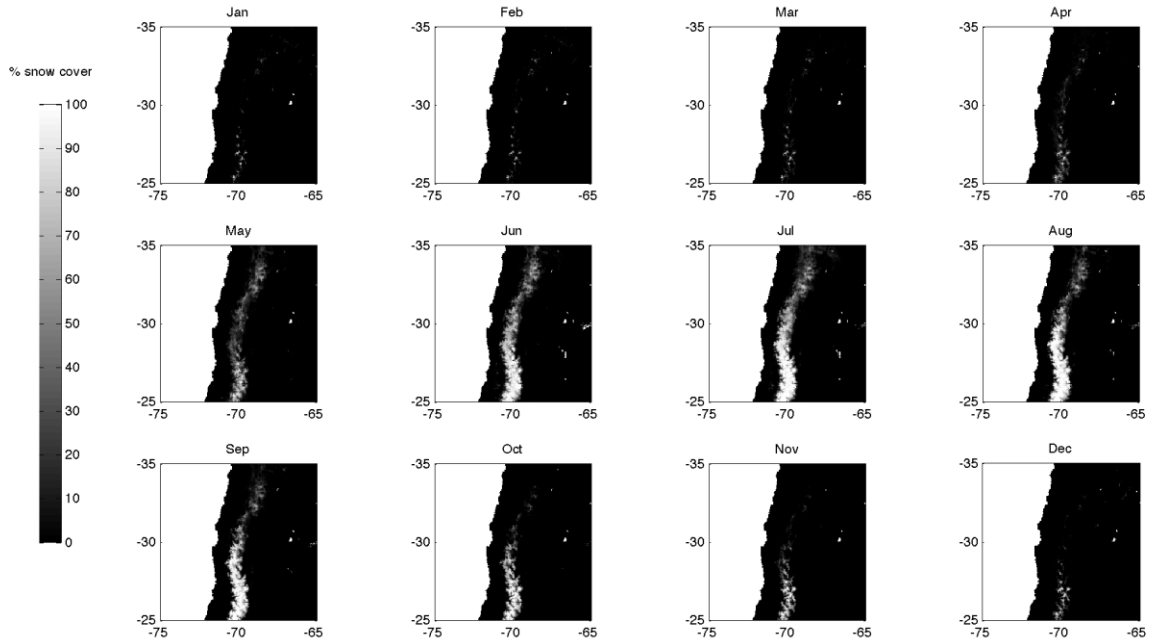
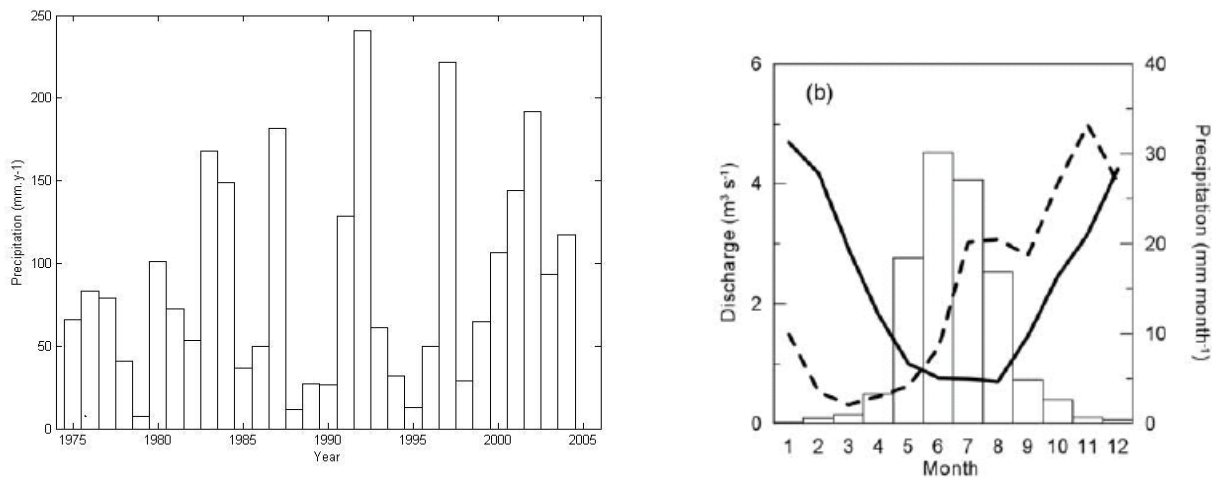


Figure 2 - Mean seasonal snow cover area derived from MODIS satellite imagery

## 1.1. Interannual variability

Another characteristic of the region is the uneven distribution of precipitations amounts throughout the years due in part to the El-Niño Southern Oscillation (ENSO) phenomenon (Figure 3). For more information about the climatic context of the Andes the reader can refer to the review of Garreaud [2009], and more specifically to the region of Norte Chico to Favier and al. [2009].



**Figure 3 – (a) - Annual Precipitation at La Serena (Id 32 – see Figure 1) between 1975 and 2005. (b)- Seasonal variation of precipitation and discharge in Norte Chico region. The open bars are mean monthly precipitation between 1900 and 2005 at La Serena (Id 32 – table of precipitation gauges in annex and Figure 1 above). The continuous line is mean monthly discharge at La Laguna Embalse (Id 11 – see table of runoff stations in annex) between 1964 and 2005. The dashed line is mean monthly discharge of Hurtado River at Recoleta Dam (Id 24) between 1928 and 1984 (from [Favier *et al.*, 2009]).**

## 1.2. Hydrology in mountainous areas

The region being dominated by mountainous areas, the hydrological situation of the Norte Chico is particularly complex. There is a wide range of papers that deal with the specific difficulties of hydrology in the mountainous catchments (spatial and temporal variability, measure network, snow under-catch), so we will not insist more in this document on that point [Klemes, 1990]. Among those, a lot of studies aim to develop a method for estimating the distribution of precipitation [Benichou and Le Breton, 1987] [Buytaert *et al.*, 2006] [Goovaerts, 2000] [Clark and Slater, 2006] [Gottardi, 2009], but this issue remains a challenge for hydrologists (see for example the review by Valery [2009]). The main problem is that it is simply impossible to observe the mean areal precipitation itself [Valery *et al.*, 2009a]. To avoid the difficulties of estimating directly the areal precipitation in mountain catchments, some authors have proposed to use the water balance formula to assess the areal precipitation in a way of inverting the hydrological cycle [Valery *et al.*, 2009b] [Weingartner *et al.*, 2007]. The motivation is that the catchment is the only system to know the mean areal precipitation it receives. Yet, this method requires estimating precisely the components of the water balance like evaporation and change in water storage.

In the Norte Chico both precipitation and discharge are poorly monitored in high altitudes (>3000 m above sea level (a.s.l.)) because they are most of the time inaccessible and covered by snow during winter. There is no precipitation gauge above 3100 m a.s.l., although 33 % of the region territory is located above this altitude. Considering the 75 available rain gauges records over the study area, the density of the measure network is close to 1550 km<sup>2</sup>/precipitation gauge, while the World Meteorological Organization (WMO) recommends 250 km<sup>2</sup>/precipitation gauge in mountainous areas [Viviroli and Weingartner, 2004] and only a small number of the stations are located in high altitudes.

## 2. Presentation of previous studies and methods for estimating the spatial distribution of precipitation

Here are presented briefly an inventory of previous works proposing a spatial distribution of precipitation over the Norte-Chico region. The work of Souvignet [2007] about the hydrology of the Elqui watershed and the paper of Favier and al. [2009] are the two most relevant available published studies.

### 2.1. Interpolation models based on fields observations

Despite the fact that water is essential to local economy in this semiarid region, there are only a few previous studies similar to this work. Their authors rely above all on the precipitation gauges data.

#### 2.1.1. Basic interpolation models

##### 2.1.1.1. The Thiessen polygons method

The Thiessen polygon area based weighted scheme has proven to perform badly in the Elqui watershed [Souvignet, 2007]. In general, it is well known that it does not simulate well the complicated topography and the different precipitation patterns observed in high-altitude, because as a univariate method it does not account for the effect of altitude. We will not insist more on this method in the following.

##### 2.1.1.2. The isohyets method

Souvignet [2007] presents a spatial distribution of precipitation relying on the isohyets method. The method is applied to the Rio Claro watershed for the period 1990-2000 at a daily timestep. It is then used as an input of a semi-lumped watershed model running on a daily timestep and was not itself tested for validation since the validation step was applied here on the rainfall-runoff model. The isohyet method is an interpolation method relying on precipitations gauges data. As such, it theoretically does not allow the estimation of precipitation rates higher than the maximal observed value. In it is not specified how is extrapolated the precipitation in high-altitude areas symbolized in red on the map below (Figure 4) extracted from the thesis of Souvignet [2007]. The elevation-precipitation dependency may somehow be included but this information is not specified.

Figure 20: Isoyets for the Elqui and the Claro Watersheds. [Source: after data provided by the DGA and CEAZA]

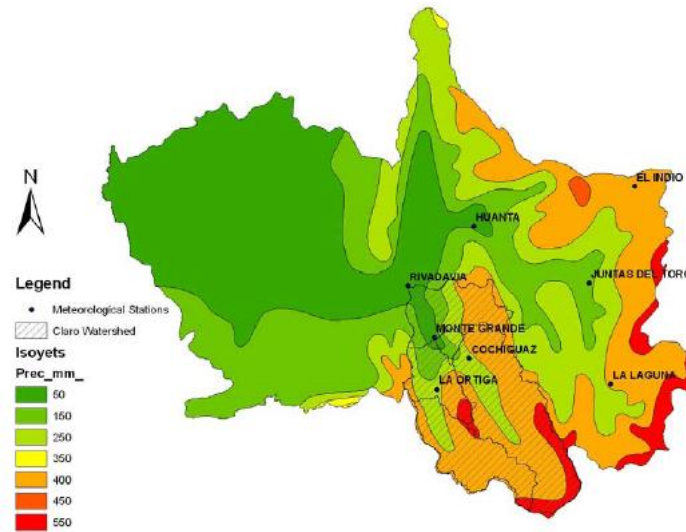


Figure 4 extracted from [Souvignet, 2007] – Isohyets for the Elqui Watershed after data provided by the DGA and CEAZA

### 2.1.1.3. A simple interpolation scheme

Over the entire Norte Chico region, Favier and al. [2009] applied a simple interpolation scheme to distribute precipitation per catchments. Considering two catchments  $S_1$  and  $S_2$  (Figure 5),  $P_1$  is considered as representative over  $S_1$ , while over  $S_2$ , the mean of  $P_2$  and  $P_2'$  will be considered, except in the part occupied by  $S_1$ .

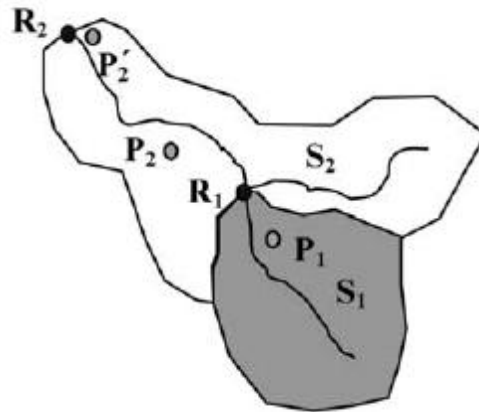


Figure 5 extracted from [Favier et al., 2009] - Example of the methodology used to estimate catchment scale precipitation

## 2.1.2. Geostatistical approaches

### 2.1.2.1. Inverse Distance Weighted interpolation method (IDW)

This method is reputed reliable and robust and can be applied without too much biases on complicated topography regions. This method is straightforward and was used for the ongoing master thesis dealing with the hydrology of the Elqui and Limari basins supervised by Drs H. Jourde, [Blanc, 2009] [Rochette, master thesis in progress] [Brisset, master thesis in progress]. The

distribution of precipitation is here used in input of a hydrological model. It is not a goal in itself but only a necessary step part of a larger task.

### 2.1.2.2. Elevation dependency in geostatistical approaches

A geostatistical approach for incorporating elevation into the spatial interpolation of rainfall has been used by Morales and al. [2004]. More specifically, a comparison of different methods for interpolating the climatological variables has been done, including ordinary kriging, block kriging (both stochastic geointerpolation models) and statistic regression based geointerpolation methods. Precipitation is here calculated as a function of geographic variables as altitude, geographic coordinates or distance to coast (Figure 6). In this study, the performance of each interpolation procedure was not presented, apart from some qualitative comments.

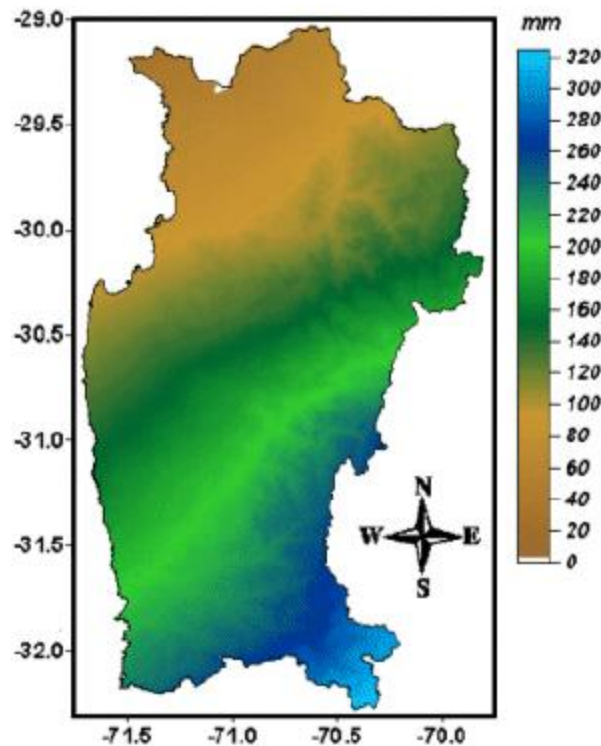


Figura 4. Precipitación media anual en milímetros.  
Figure 4. Mean annual rainfall in millimeters.

Figure 6 – Spatial distribution of precipitation over Coquimbo region computed by multiple regression, from [Morales et al., 2004]

Kriging requires the analysis of the variogram to fit a variogram model. In our case, it would mean that each of the 384 variogram (1 per month) should be analyzed and fitted. Automatic fitting of variogram is generally not recommended. Therefore, kriging does not seem to be an appropriate technique and was not considered in this work.

## 2.2. Consideration of atmospheric prediction model

After demonstrating that the low accuracy of mean annual areal precipitations obtained by a simple interpolation explains discrepancies between discharge and precipitation in high-altitude

areas of Norte Chico region, Favier and al. [2009] employed atmospheric models (global<sup>1</sup> and regional<sup>2</sup>) to derive spatial distribution of precipitation. The use of GFS precipitation led to better closure of the water balance for most high-altitude catchments.

### 3. Description of the data and the orographic correction factor method

#### 3.1. Data

##### 3.1.1. Precipitation gauges and runoff stations

The study is principally based on monthly precipitation from 75 precipitation gauges (Table 10 in annex) and runoff records from 56 river gauging stations (Table 11 in annex) of Norte Chico region. Data were provided by Chilean national water management institution (DGA)<sup>3</sup> and meteorological institute (DMC)<sup>4</sup>. The stations are located, south to north, in the watersheds of Choapa, Limari, Elqui, Huasco and Copiapo rivers. Data availability varies between stations, from a few years to nearly one century for the longest record of precipitation. The study of the long-term precipitation and discharge variability is not a priority in this work (for this, the reader can refer to [Favier *et al.*, 2009]). We only used the data collected between 1975 and 2006 because the time series are very sparse before 1975. The quality of the data was not questioned. We assumed that quality checks were previously performed by both institutions. Two limits are remaining. First, the precipitation gauges located in altitude are subject to snow under-catch in the wintertime when precipitations occur as snow. Second, the Norte Chico rivers discharge may be affected by agriculture activity through the network of regulation dams and irrigation channels. The possibility of biases in the discharge data in areas below 2000 m a.s.l. is therefore important.

##### 3.1.2. Snowfall measurement and snow water equivalent

Observation data of snow accumulation were used to validate the spatial distribution of precipitation in high-altitude. They are subjects to possible biases related to the snow water equivalent conversion. The Snow Water Equivalent (SWE) is defined as the amount of water contained within the snowpack (Resources Conservation Service (United States Department of Agriculture)). Some specific-designed network have been installed to monitor snowfall in regions where hydroelectricity is generated (EDF in France, see [Gottardi, 2009]) and sometimes an ultrasonic snow depth sensor may be used (for example the automatic weather stations of CEAZA at Pascua-Lama) but most of the time, the SWE measurement relies on manual measurements on the field along a line of several hundred meters known as snow courses. The main difficulty remains that the snowpack is transforming throughout the time: the density changes and melt can occur. The observations can only reflect the state of the snowpack at the moment of the observation. The more frequent the measurements are accomplished the more confidence in estimating the water volume is permitted. In the Norte Chico, the majority of snow water equivalent measurements are bi-annual and there is no way to be sure that the whole snow accumulation has been recorded.

---

<sup>1</sup> Global Forecast System (GFS)

<sup>2</sup> Weather Research and Forecasting (WRF)

<sup>3</sup> Dirección General de Aguas

<sup>4</sup> Dirección Meteorológica de Chile

### 3.1.2.1. Available data

Available snow water equivalent measurements are sparse and come from two different sources. The first one is the national water management institution (DGA) that is in charge of estimating the volume of fresh water available each year. This is used to anticipate reservoirs management and to attribute the water rights to users. The second one comes from the mining companies which are located in high-altitude areas. Snowfall monitoring is required for their own activity but also, and more recently, because they are committed to environmental monitoring (Pascua-Lama). These measurements were not included into the data set used for cross-validation and interpolation of precipitation for two reasons. First, we need “fresh” data for validation i.e. that are independent from data used for model calibration. Second, we preferred keeping the homogeneity of the data set used for both the interpolation and the validation. This is particularly true because precipitation gauges measure the volume of water directly while SWE is derived from snow depth measurements using the snow density and thus introducing a new source of uncertainty. For all but one SWE records, the water equivalent was available. For the site Pascua-Lama (Id 2, see Table 1 below), only snow depth measurement was available. We considered the mean annual snow density provided by the measurements of the site El Indio (Id 1, see Table 1). We used SWE measurements from seven snow courses (Figure 7). The data are heterogeneous (Table 1). In particular, the maximum of snow accumulation may be biased some years as the measurements were carried out only once a year. The protocol requires that the snow course is done whenever the maximum of snow accumulation has been reached, but the reality may differ. A more detailed analysis on the accuracy of SWE data is out of purpose in this work but it is likely that the uncertainty on SWE is significant.

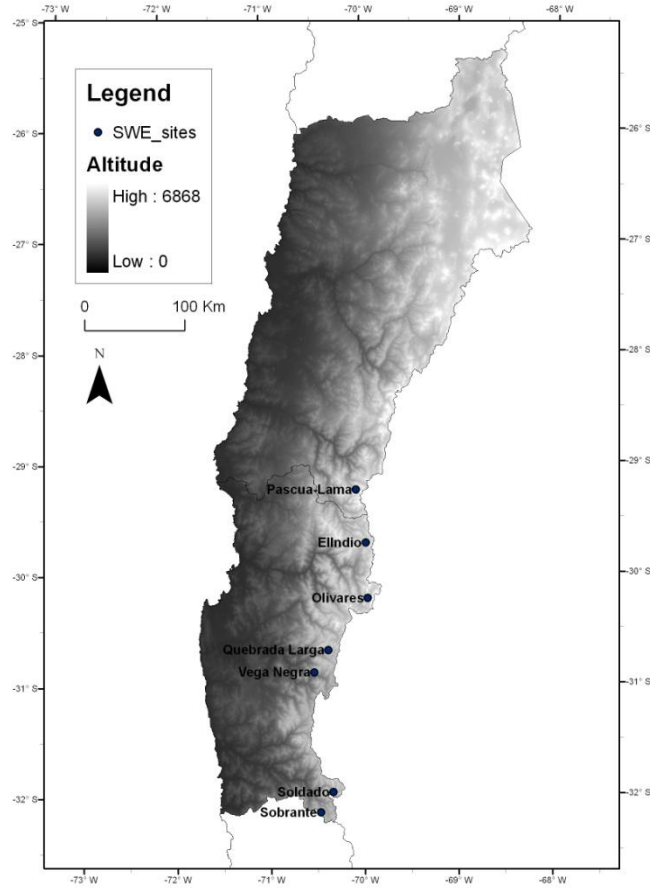


Figure 7 - Localization of available snow water equivalent measurement sites

Id_Snow	Name	Source	Time-Step	Period	Lon	Lat	Alt (m)	SWE_Obs (mm/y)
1	El Indio	Mining Co.	monthly	1981-2004	-69,97	-29,75	3869	172
2	Pascua-Lama	Mining Co.	monthly	2001-2009	-70,07	-29,27	3717	179
3	Vega Negra	DGA	variable	1975-2005	-70,52	-30,92	3600	538
4	Quebrada Larga	DGA	variable	1975-2006	-70,37	-30,72	3500	328
5	Soldado	DGA	variable	1979-2006	-70,33	-32,00	3200	456
6	Olivares	DGA	variable	1975-2006	-69,95	-30,25	3550	149
7	Sobrante	DGA	variable	1981-2000	-70,47	-32,18	3250	437

Table 1 - Snow Water Equivalent (SWE)

Another set of data from DGA were used. It provides daily snow water equivalent measurements for three sites over the period 2000-2008. We do not have further information about the measurement protocol and there are some gaps in the data. Yet, we assumed that these observations are reliable and that we can use them to test the different methods of interpolation. We first aggregated the daily observations to annual snow accumulation. The Figure 8 shows an example of this kind of data. The vertical line represents the water equivalent in millimeters of the snowpack throughout the year 2008. The snowpack exists between May and November.

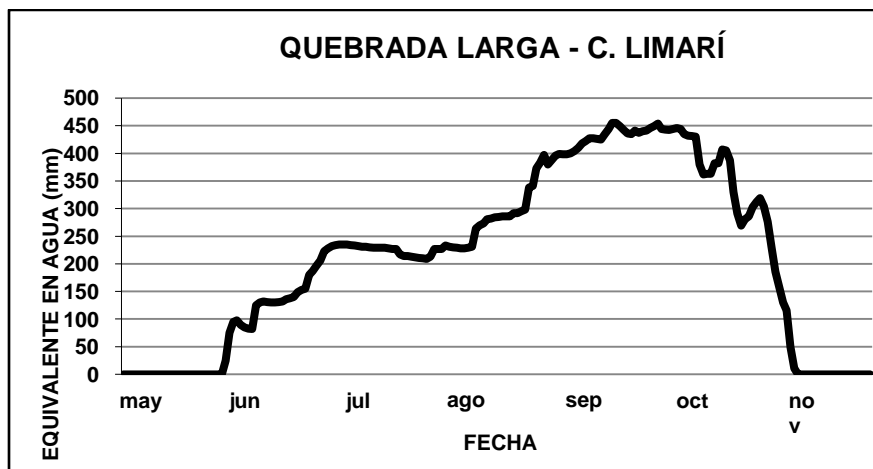


Figure 8 - Example of daily snow water equivalent measurements provided by DGA. Here is plotted the snow accumulation in Quebrada Larga (see table below to localisation) in the year 2008. In our analysis, the intermediate melts have been taken in count. The SWE is thus taken as the maximum of the vertical line plus the intermediate melts.

### 3.1.3. Remote sensing data

Remotely sensed data relying on ground-based radar and satellite imagery is a developing alternative way to assess rainfall over a region. The major limit of these technologies for now is the relative poor resolution they offer. The consideration of this data is indeed possible only working on middle or large scale, when on the contrary a densely gauged catchment allows us a thin resolution. Yet we must recognize that so well instrumented catchment are seldom and that remotely sensed data can therefore in many cases be a precious help to improve the knowledge of precipitation over regions. Remote detection data have been used to assess the snow cover area (MODIS)<sup>5</sup> and to test an alternative method of precipitation estimation (TRMM)<sup>6</sup>.

#### 3.1.3.1. Satellite imagery

The satellite imagery from MOD10CM was used to assess to snow cover area (4.4.2.2). MOD10CM is a binary estimation (snow/no snow) with a 0,05° spatial resolution. We studied monthly variation of snow extend between 2000 and 2009.

#### 3.1.3.2. The Tropical Rainfall Measuring Mission project (TRMM)

TRMM is a joint mission between the National Aeronautics and Space Administration (NASA) and the Japan Aerospace Exploration agency (JAXA) designed to monitor and study tropical rainfall (<http://trmm.gsfc.nasa.gov/>). The main instrument aboard is a precipitation radar providing information on the intensity and distribution of rain as well as the rain type or the height at which the snow melt into rain. The data we used are freely available and provide precipitation estimations with a monthly time step over the period 1998-2009 and with a 0,25° resolution. These data were used in order to compare two approaches for estimating the distribution of precipitation over the study area: the orographic correction factor method based on field observations and the method derivated of TRMM data based on remote sensing.

<sup>5</sup> Moderate Resolution Infrared Spectrometer

<sup>6</sup> Tropical Rainfall Measuring Mission

### 3.1.4. Digital Elevation Model

We disposed of a high-resolution SRTM<sup>7</sup>-based DEM of Chile provided by CEAZA (resolution of 0,001°). Since such a thin resolution is not accommodated for the precipitation interpolation, we chose a less refined DEM (source: CEMAGREF, centre d'Antony, HBAN) which covers the entire Earth surface and extracted the region of Norte Chico. The resolution of this DEM is 0,01°.

### 3.2. Elevation-dependent regionalization method

We searched a parsimonious model that could estimate as well as possible the precipitation in each point of the region based on the observations provided by the precipitation gauges network. The assumed elevation dependence of precipitation in the study region made us look for a new method that aims to improve the areal estimation of precipitation on mountainous catchments [Valéry, 2009]. This method is designed to rely on both the neighborhood and a multiplicative correction of amounts of precipitation based on the difference of altitude between a target and the neighbors.

- The neighborhood is a widely used concept in interpolation. The more the observation stations are close to each other, the more the observations are correlated. For a specified target (the point where we want to estimate the precipitation) the term neighborhood designates all the precipitation stations that will be included in the calculation of the estimations at the target point. We adopted in this method the inversed distance weighting procedure. The more the station is close to the target, the more his weight in the calculation is high. The distance is computed as the so-called great-circle distance, which is the shortest distance between two points on the surface on a globe, here the Earth. Distance calculations are made in spheric system.

$$\omega_{target, neighbour} = \frac{1}{(distance_{target, neighbour})^\alpha} \quad (\text{Equation 1})$$

- The correction of precipitations aims to reproduce the relationship between the precipitation and the relief by introducing an orographic correction factor  $\beta_{alt}$  ( $m^{-1}$ ). A multiplicative correction method was chosen, which is considered better adapted to a discontinuous phenomenon, bounded by zero. Indeed, it avoids the threshold effect of a subtractive model and the exponential formulation allows the symmetry of the transfer of information. The contribution of one of the neighbors for the estimation precipitation in the target point is calculated as follows.

$$P_{target,neighbour} = P_{neighbour} \times \exp[\beta_{alt} \times (z_{target} - z_{neighbour})] \quad (\text{Equation 2})$$

The parsimonious method, only two parameters, quickly described below, needs to be calibrated. That will be done through a process of cross-validation as presented in the following part.

---

<sup>7</sup> Shuttle Radar Topography Mission

### 3.2.1. The calibration of the model – Cross-validation by jack-knife procedure

The cross-validation process enables to calibrate the parameters of the model by trying to reproduce as faithfully as possible the precipitation in each observation gauge thank to his neighborhood. We used a specific form of cross-validation known as jack-knife procedure. Each precipitation gauge is banished from the data set in turn. This new set of data forms the neighborhood of the banished precipitation gauge (the target). It is then used to predict precipitation at the target. The monthly estimation at the target was calculated as follows:

$$P_{m,target}^{sim} = \frac{\sum_{neighbor}^{Nstats} [\omega_{target,neighbor} \times P_{m,neighbor}^{obs} \times \exp[\beta_{alt} \times (z_{target} - z_{neighbor})]]}{\sum_{neighbor}^{Nstats} \omega_{target,neighbor}} \quad (\text{Equation 3})$$

For each precipitation gauge, we disposed thus of two records, one of observations and other of simulations. These records have been compared in the frame of efficiency functions, leading to the characterization of the optimized parameters  $\alpha$  and  $\beta_{alt}$  by trial and error.

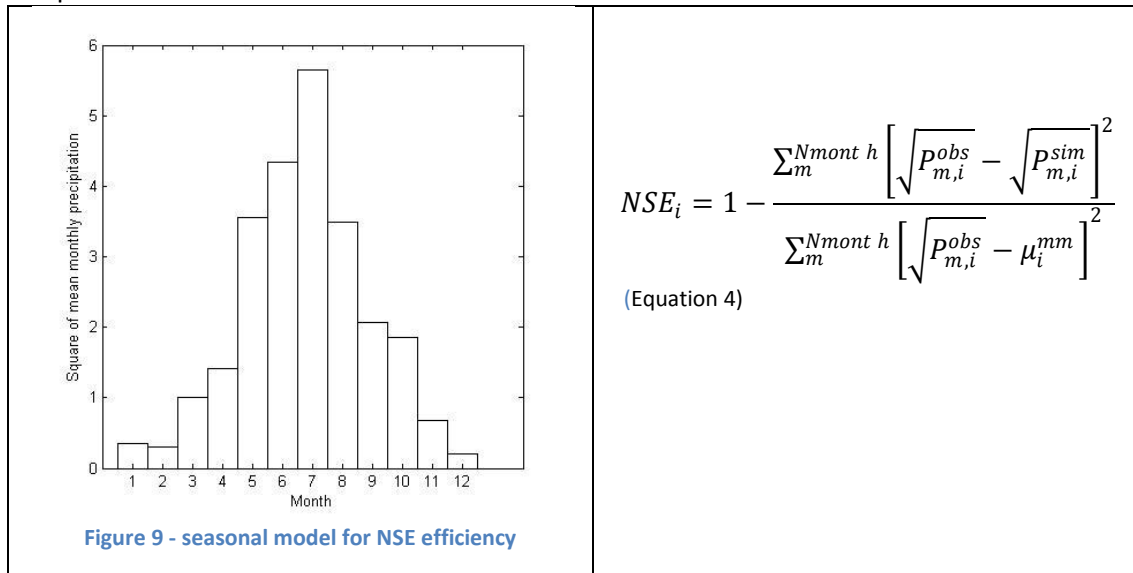
The gaps in data records and the strong seasonality of precipitations make us look to an accurate mode for calculate the annual mean of precipitation. Over the period 1975-2006, the monthly cycle of precipitations is first calculated. The mean annual precipitation  $P$  is then the sum of the monthly amounts of precipitations previously obtained. This mode of calculation is of course applied the same way for both the observations and the estimations. We calculated thus  $P^{obs}$  and  $P^{sim}$ .

### 3.2.2. Efficiency functions

Different efficiency functions were used to calibrate the model.

#### « Seasonal » Nash-Sutcliffe (NSE) efficiency

This efficiency function is quite elaborated since we introduced here the seasonality in the sparring partner model (Figure 9). The root-square operation attenuates the influence of major precipitation amounts relative to months of little precipitation.  $\mu_i^{mm}$  is a vector of 12 elements, a value per month.



### **Kling-Gupta (KGE) efficiency [Gupta et al., 2009]**

The authors showed how model calibration problems can arise due to interactions among the components of the NSE [Gupta et al., 2009]. This alternative criterion has been used as we assume that it may improve the evaluation of model performance.

$$KGE_i = 1 - \sqrt{(r - 1)^2 + (a - 1)^2 + (b - 1)^2} \quad (\text{Equation 5})$$

Where,

$r$  is the linear correlation coefficient between  $P_{m,i}^{sim}$  and  $P_{m,i}^{obs}$

$a$  is the standard deviation of  $P_{m,i}^{sim}$  divided by the standard deviation of  $P_{m,i}^{obs}$

$b$  is the mean of  $P_{m,i}^{sim}$  divided by the mean of  $P_{m,i}^{obs}$

### **The Bias**

Calculated over a large period, it identifies a mean underestimation or overestimation.

$$Bias_i = \frac{\sum_m^{Nmonth} P_{m,i}^{sim}}{\sum_m^{Nmonth} P_{m,i}^{obs}} \quad (\text{Equation 6})$$

## 4. Results

### 4.1. Characterization of the model parameters

#### 4.1.1. Results of optimization

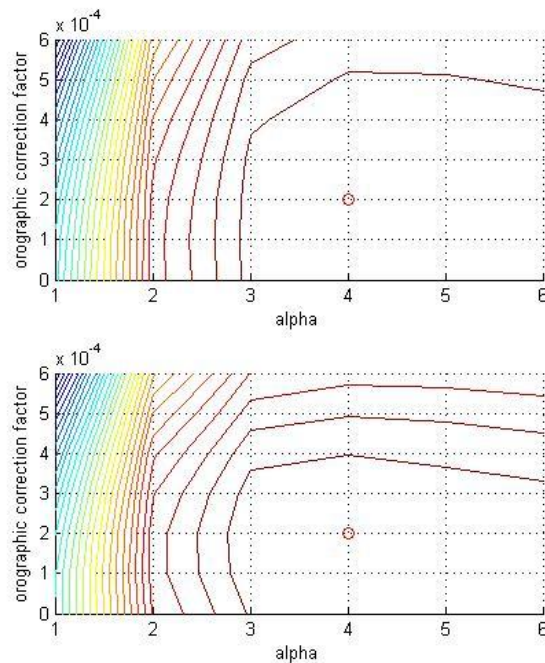


Figure 10 – Efficiency of different sets of parameters in cross-validation. The figure above represents the NSE efficiency while the figure below represents the KGE efficiency.

The trial-error process is conducted with entire values from 1 to 8 for  $\alpha$  and values from 0 to  $6 \cdot 10^{-4}$  with a scale of  $0,1 \cdot 10^{-4}$  for  $\beta_{alt}$ . The period of calculation is set to January 1975 – December 2006. The Figure 10 presents the lines of equal performance respect to the cross-validation for the two main criterions: NSE and KGE. The red circle refers to the set of parameters where the performance is the best.

For both the NSE and the KGE, the set of optimized parameters is composed of  $\alpha = 4$  and  $\beta_{alt} = 2,2 \cdot 10^{-4} \text{ m}^{-1}$ . The criterion of bias looks to be less sensitive to the set of parameters as soon as  $\alpha$  is set greater than 3. Indeed, with  $\alpha > 3$ , the bias is always included between 1 and 1,1 whatever the value set for orographic correction factor .

The Figure 11 following does not show a dependence of efficiency functions with the altitude, but the little number of gauges located in altitude does not make this identification easy.

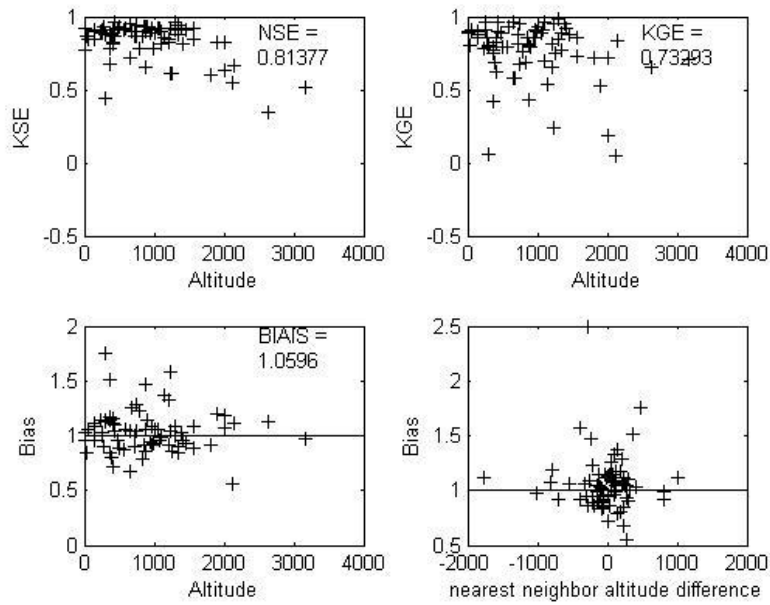


Figure 11 - Performances at precipitation gauges in cross-validation

#### 4.1.2. Attempts to improve the orographic correction factor model

Some typical attempts to improve the identification of the elevation-dependent relationship are investigated.

##### 4.1.2.1. A spatial distribution of orographic correction factors

The spatial-dependence in different scales of orographic correction factor is a largely discussed point. First, the correction factor can be defined from a local scale (one value per mesh) [Gottardi, 2009] to a national scale (one value per country) [Valéry, 2009] passing by a regional scale (one value per massif). Second, the orographic correction can depend on the altitude. Some authors have underlined the difficulty to identify orographic correction factors above a threshold of altitude [Ranzi, 2009] and observed possible inversion of orographic correction factor with the altitude [Barry, 2008]. Thus uncertainties about identifying the orographic correction factor increase with altitude. We test the introduction of a threshold. Above this threshold, the corrections remain the same. The results do not show significant impacts. Moreover, in Norte Chico region, despite the lack of stations above 3100 m a.s.l. the orographic enhancement is supposed to continue to higher altitudes [Favier et al., 2009].

Next, the jack-knife methodology is computed separately over each watershed (Table 2).

Valley	Choapa	Limari	Elqui	Huasco	Copiapo
$\beta_{alt}$ ( $\cdot 10^{-4} m^{-1}$ )	1	2	2	4	4
Gauges number	19	22	13	7	8
$Z_i_{max}$ (m a.s.l)	1250	2640	3100	1900	2115
$Z_i_{min}$ (m a.s.l)	10	134	15	150	370

Table 2- Optimized orographic correction factor for each watershed

Despite this regionalization, we observe that the global performances of the model are not affected. The orographic correction factor previously identified is still a regional one.

#### 4.1.2.2. A seasonal distribution of orographic correction factors

Due to the strong seasonality of precipitation over the region, we may improve our model by introducing a seasonal distribution of orographic correction factors. The distribution of monthly optimized orographic correction factor (alpha is set to 4) is presented in Figure 12 below.

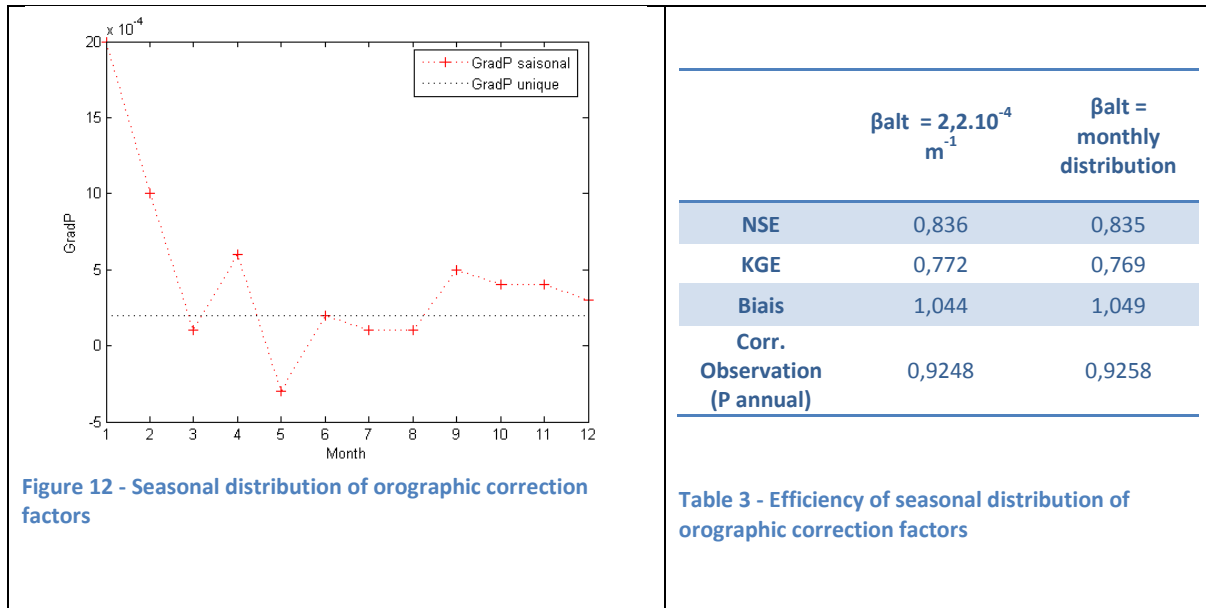


Figure 12 - Seasonal distribution of orographic correction factors

Table 3 - Efficiency of seasonal distribution of orographic correction factors

First, we observe that in general, the correction factor is bigger for the months with little precipitation (ONDJF) and for the rainy months (JJ), the correction factor is not very different that the global one previously computed ( $2,2 \cdot 10^{-4} \text{ m}^{-1}$ ). This distribution is then used to compute the estimation precipitation over the rain gauges, but we must keep in mind that the monthly orographic correction factors for the very dry months are poor constrained and thus subject to a doubtful meaning.

For now, the introduction of seasonality in the orographic correction factor does not seem to have a strong impact over the model as seen in Table 3. Moreover the physical meaning of this seasonal distribution is difficult to asses. The important values of winter months may be explained by the discrepancies between the summer precipitation events frequency in low and high altitudes catchments [Favier et al., 2009]. They may also come from episodic rainfall events in summer in high-altitude known as events of *invierno boliviano*.

#### 4.1.2.3. Impact of ENSO

We examine here the influence of the El-Nino Southern Oscillation (ENSO) that is a climate pattern that occurs on average every five years and well-known for its association with floods, droughts and other weather disturbances in the region of Norte Chico. The influence of ENSO is observed by the following way: for each year of the period 1975-2006, we compute the optimized orographic correction factor and the associated efficiency and look for a relationship between these results and the index ENSO. The Figure 13 does not show any relationship between the correction factor and the index ENSO.

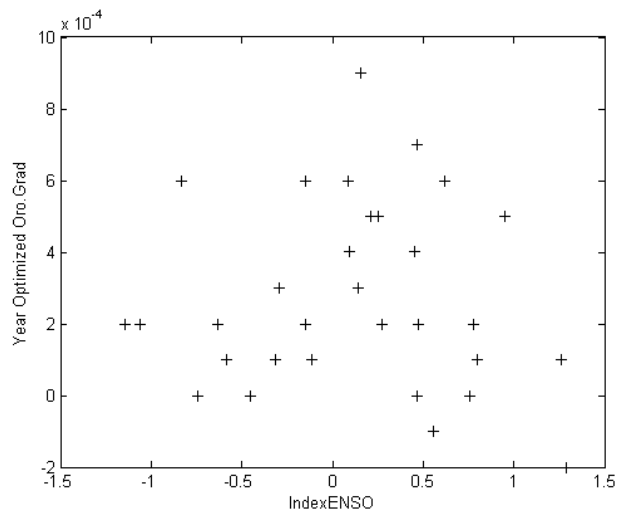


Figure 13 – Relationship between annual optimized orographic correction factor and ENSO

#### 4.1.2.4. The weather-dependence

Eventually, we should focus on the relationship between the orographic correction and the intensity of a precipitation event. If the analysis show significant results, we may be able to introduce a new dependence over the orographic correction factor based on the weather (for example: no precipitation/small event/medium event/huge event). Here, since we are working on monthly precipitation, this analysis is out of sense. Moreover the dependence of orographic correction factor with the intensity of rain is included in the seasonality like described above. Thus, we will not investigate more in this direction. But it is interesting to look both at the study of Valery [2009] who observed a negligible impact of the weather and the work of Gottardi [2009], who on the contrary founded his model on a weather-dependence of the orographic correction factor.

#### 4.1.2.5. Conclusions

The lack of available data in the study region may explain why the attempts to better asses the orographic correction factor failed. Moreover the the first results of spatial distribution of precipitation reveal some incoherencies using a monthly distribution of orographic correction factors or a threshold for altitude. Valery [2009] went to the same conclusions after a fine inquiry of the same possible enhancements of the method.

### 4.2. First level of validation – Cross-validation

Some examples of the monthly predictions calculated thank to the jack-knife methodology are shown in Figure 14.

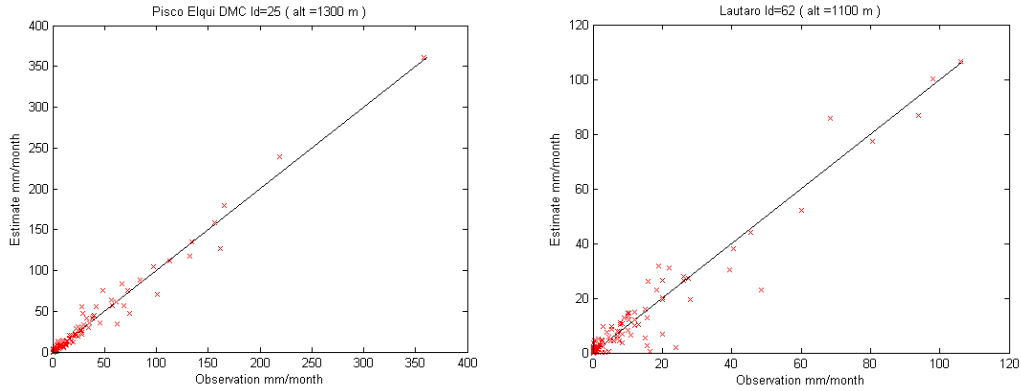


Figure 14 – Scatter plots of monthly precipitation observations (bottom axis) and estimations (left axis) at Pisco Elqui (Id 25 – Elqui Valley) and Lautaro (Id 62 – Copiapo Valley).

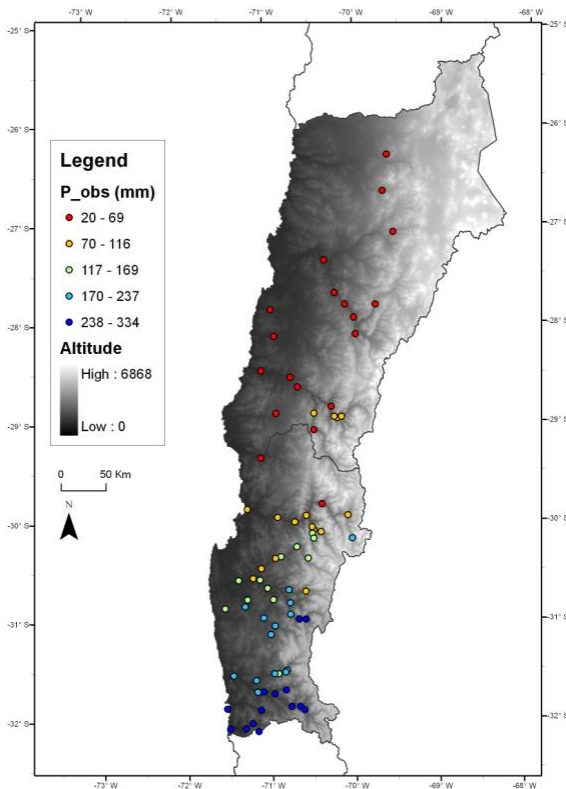


Figure 15 – Mean annual precipitation observation  $P^{obs}$  at precipitation gauges.

The Figure 15 and Figure 16 present the mean annual precipitation at gauges ( $P^{obs}$  and  $P^{sim}$ ).

The relative bias presented below is calculated as follows:

$$Relative\ Bias = \left| \frac{(P^{sim} - P^{obs})}{P^{obs}} \right|,$$

where  $P^{sim}$  and  $P^{obs}$  are both mean annual precipitation. There is not any general trend to under- or overestimation in terms of annual mean precipitation. The stations corresponding to the major biases were identified and analysed separately:

The station Los Molles (Id 54) is the most biased with 65% of overestimation. The analysis of the record reveals a large number of gaps within a short record of only 8 years. In particular, the winter wet months (JJA) are poorly monitored since only 2 or 3 years of observations are available. The mean annual precipitation  $P^{obs}$  (54) is therefore reputed doubtful and the value is much lower than his neighbors. Yet, this gauge is not identified as an outlier and should not be removed from the set of precipitation gauge.

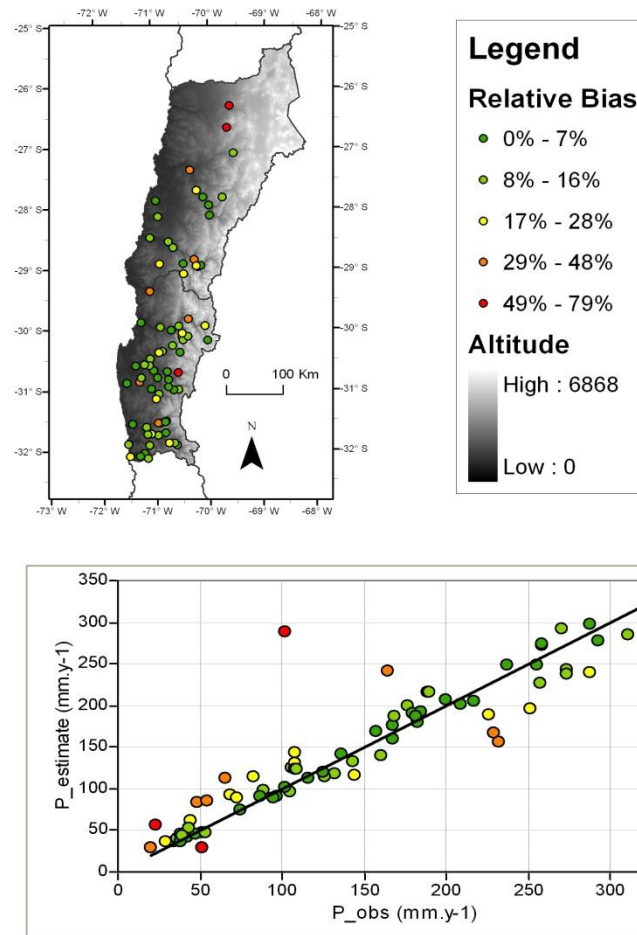


Figure 16 - Spatial distribution of relative bias and scatter plot of mean annual precipitation observation (bottom axis) and estimations (left axis). The color of circles refer to the relative bias.

The stations Huitil (Id 7) and La Canela DMC (Id 5) seem to be consistent over the period 1975-2006 but despite the fact that they are located close to each other, about 5 km, and in similar mid-altitude (respectively 650 and 880 m a.s.l.), the mean annual precipitation are quite different, respectively 232 and 164 mm.y<sup>-1</sup>. The source of records, DGA for the first and DMC for the second may explain this difference.

The mean annual observed precipitation at the station La Placilla (Id 45, 400m a.s.l, P<sup>obs</sup> = 229 mm<sup>-1</sup>, P<sup>sim</sup> = 167 mm<sup>-1</sup>) is far higher than its neighbors. Neither the altitude nor the period of observations can explain this anomaly. This results in an important underestimation (-37%).

Eventually, we should focus on the poor estimations over the two gauges located in the far North of the region, Las Vegas (Id 66) and El Salvador (Id 75). In this arid area of Atacama desert (P<sup>obs</sup> are respectively 52 and 23 mm.y<sup>-1</sup>), the climatic and precipitation variability is extreme, both spatially and temporally. Two local extreme precipitation events observed at Las Vegas (July 1984 and July 1987 with respectively 340 and 208 mm) and poorly observed at El Salvador (0 and 28 mm) may explain the estimations and large biases here.

In conclusion, the major biases (>30%) between the annual mean Pobs and Psim can be explained by the large differences of observed precipitation amounts that can occur between neighbors gauges. The fine analysis of the records did not allow us to identify any anomalies in the data so

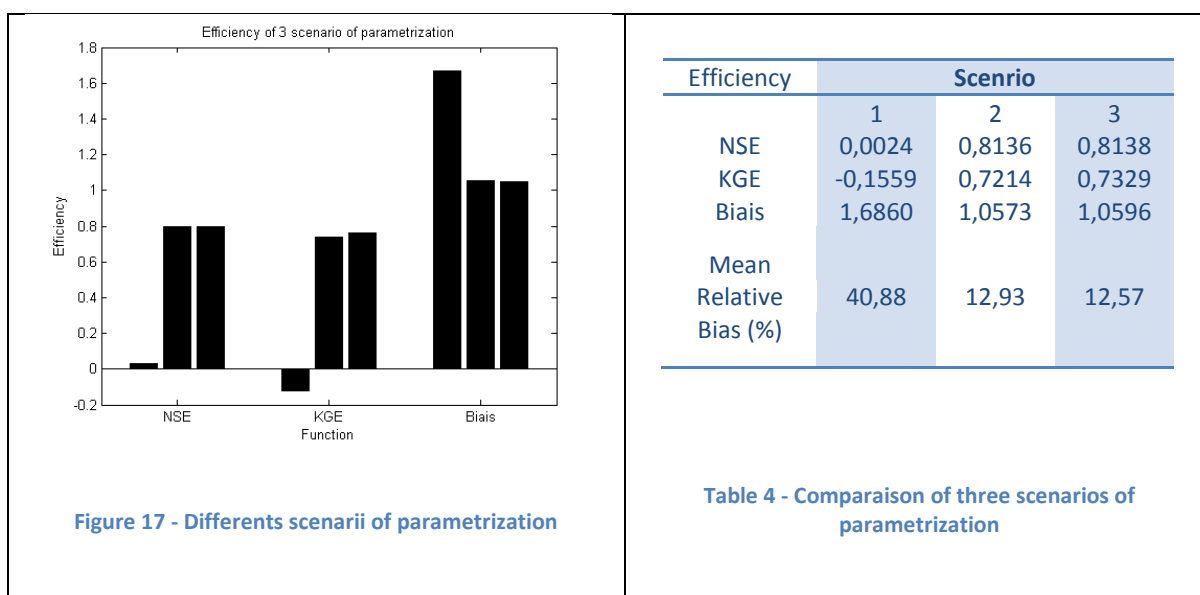
we did not remove any precipitation gauge from the dataset and the chosen period 1975-2006 remains valid.

#### 4.2.1. Discussion of the impacts of the orographic correction factor

We investigate at this first level of validation (precipitation estimation over the gauges) the relevance of the method, and in particular the impact of the orographic correction factor. In order to do this, we compare the results of the three following scenarios of parametrization:

- scenario 1:  $\alpha = 0$  et  $\beta_{alt} = 0$ , this is a set of parameters for basic interpolation.
- scenario 2:  $\alpha = 4$  et  $\beta_{alt} = 0$ , this set corresponds to a neighborhood-based interpolation.
- scenario 3:  $\alpha = 4$  et  $\beta_{alt} = 2,2 \cdot 10^{-4}$ , this is the optimized set of parameters.

The enhancement of performances is clear passing from the first scenario to the second one. The impacts of the orographic correction factor by itself (from the second to the third one) on the contrary are marginal. The scenario 2 without orographic correction factor does not present any trend to under or overestimation either. Moreover, we notice only small discrepancies between scenarios with respects to both efficiency functions and mean annual precipitation estimation. Eventually, we could believe that the impacts of the orographic correction factor should be more apparent for the high-altitude precipitation gauges. The Figure 18 below reveals that it is not true. The Figure 17 and Table 4 present the results of these scenarios in terms of functions efficiency. When focusing on the station of la Laguna Embalse (Id 21 – 3100m a.s.l.), the highest one, we can notice that the conclusions are similar (Table 5).



Efficiency	Scenrio		
	1	2	3
NSE	0,0024	0,8136	0,8138
KGE	-0,1559	0,7214	0,7329
Biais	1,6860	1,0573	1,0596
Mean Relative Bias (%)	40,88	12,93	12,57

Figure 17 - Differents scenarii of parametrization

Table 4 - Comparaision of three scenarios of parametrization

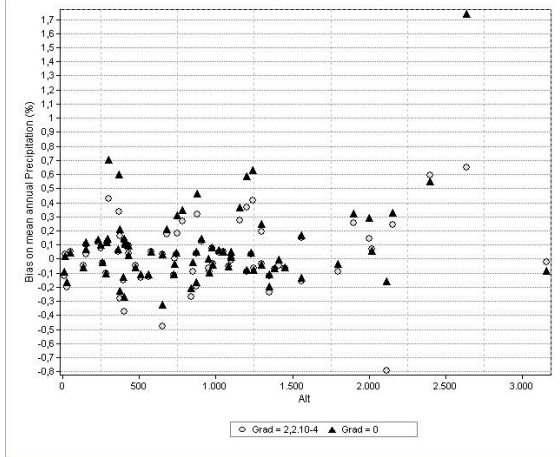


Figure 18 – Relative Bias vs Altitude for scenarios 2 (triangles) and 3 (circles)

La Laguna Embalse (3100m)		
	scenario	
	2	3
NSE	0,53	0,52
P (mm/y)	167	179
Relative Bias (%)	-9%	-2%

Table 5 - Scenarios 2 and 3 at la Laguna Embalse (Id 21 – 3100m a.s.l.)

At this step of validation, the model is dominated by the parameter of neighborhood. As a consequence, the introduction of an orographic correction factor increases only a little bit the accuracy of precipitation estimations at precipitation gauges. In particular, it does not bear on high-altitude points more than other ones. For now, the method seems thus not better than a classical inverse distance weighted one. Finally, the attempts to improve the identification of the orographic effect have failed to enhance the performances of the model.

Before computing the spatial distribution of precipitation, we investigate why the introduction of the orographic correction factor is here pointless.

Valery [2009] went to similar conclusions for one of the region she studied: Canada. On the contrary of the other ones, this region presents a moderate topography and above all a network of precipitation gauges very loose (5770 km<sup>2</sup> per gauge while 110 to 720 for the other regions (France, Switzerland and Sweden). Moreover, the sensitivity analysis in regards to the network density she accomplished revealed the limits of the method. With a more than 30% of original density decrease, the performances decrease and the altitudinal corrections can change strongly. Thus, the low density of the network of precipitation gauges in the Norte Chico region may be a first reason to the poor impact of orographic correction factor we observed in cross-validation. A basic sensitivity analysis revealed that in our case, the characterization of the optimized parameters set was dependantless of network density to the point of a 50% decrease. After, the optimized factor becomes negative and the performances sink. Testing the impact of an increase in network density is not possible.

A second reason could originate from the bias on precipitation measurements. It is well known that solid precipitation amounts are underestimated by precipitation gauges (snow undercatch). This is true in particular for the high-altitude gauge since the ratio solid precipitation/total precipitation increases with altitude. Thus, the orographic correction factor optimized with underestimated precipitation amounts in altitude may be lower. Valery et al. [2009b] suggested the introduction of a new parameter for snow undercatch correction and underlined the strong interaction with the orographic correction factor.

A third reason could be the spatial distribution of precipitation gauges. Those are indeed located along the valleys, with an East-to-West direction. The strong South-to-North gradient of precipitation can explain the high value of the neighborhood parameter ( $\alpha = 4$ ). Thus, according to

the orographic gradient from coastal areas to the cordillera, the precipitation estimation at a station is mostly constrained by its closest neighbors upstream and downstream. So there is a form of balance between the neighbors located downstream which present lower amounts of precipitation and those upstream with higher precipitation. As producing the same effect, this balance is presumed to substitute the orographic correction factor.

That is why the same directions of the spatial distribution of precipitation gauges and of the orographic and the precipitation gradients (East-West) may explain the limited influence of orographic correction factor at this step of validation.

#### 4.2.2. Spatial distribution of precipitation

The calculation is exactly the same as described for the cross-validation method, except that the targets are now each pixel of a 0,01° (around 100m) resolution grid.

The figure below (Figure 19) shows the results of the calculation for the annual mean over the period 1975-2006. As the calculation is run with a monthly time step, we dispose in reality of the spatial distribution of precipitation for each month of this period. For a month  $m$  and a pixel  $x$ , the estimation is calculated as:

$$P_{m,x}^{sim} = \frac{\sum_i^{Nstats} [\omega_{x,i} \times P_{m,i}^{obs} \times \exp[\beta_{alt} \times (z_x - z_i)]]}{\sum_i^{Nstats} \omega_{x,i}}$$

(Equation 7)

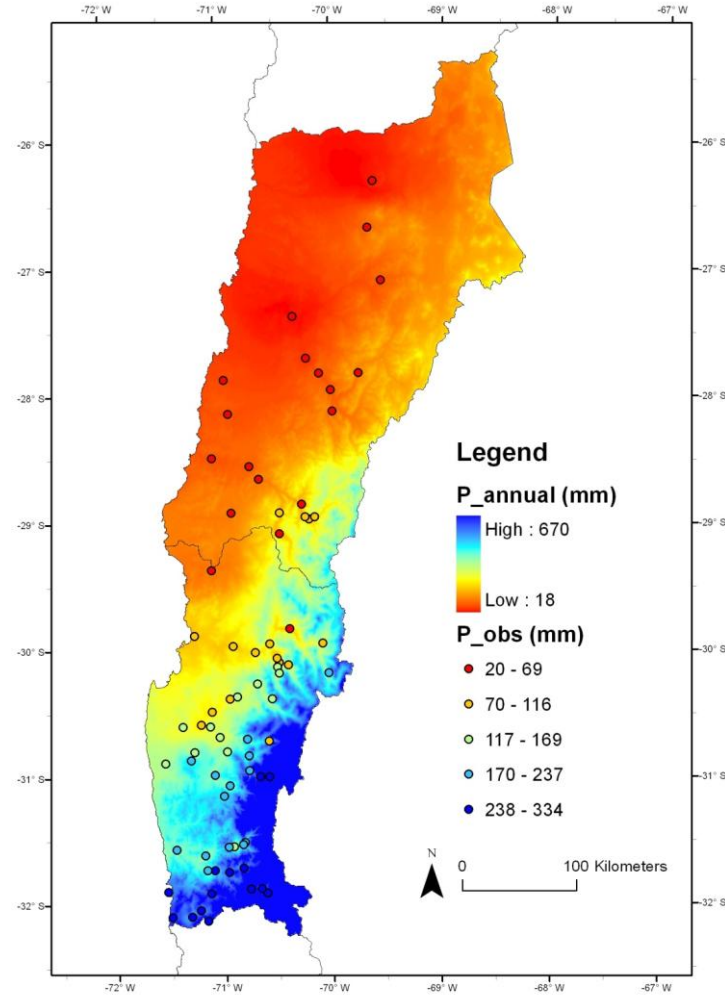


Figure 19 - Spatial distribution of mean annual precipitation computed with orographic correction factor method and mean annual precipitation observed at precipitation gauges

The southeast-northwest precipitation gradient over Norte Chico region appears clearly and the range of estimations is correct ( $18 \text{ mm.y}^{-1}$  in the region of Atacama desert and  $670 \text{ mm.y}^{-1}$  in the southern part of the Cordillera). The orographic effect is also evident.

We aim at validating the prediction in a quantitative way using independent data. Three levels of test will be investigated in turn in the following sections. First we test only the predictions over the observation points, then the estimations out of the observation network and in particular in the highest areas where both uncertainties and interest are concentrated. Eventually we compute the water budget of the catchments and testing the influence of the areal precipitation input.

### 4.3. Second level of validation: Comparison with other precipitation measurements

#### 4.3.1. Monthly TRMM predictions over precipitation gauges

The Figure 20 shows the results of the TRMM model. Again, only the distribution of annual mean precipitation over the period 1998-2009 ( $P^{\text{TRMM}}$ ) is presented.

The cell size is larger than the one of the orographic correction factor method (respectively 0,25 and 0,01 ). Yet the precipitation gradient and the range of estimations (20 – 334 mm.y<sup>-1</sup>) appear correct and similar to our interpolation results (Figure 19).

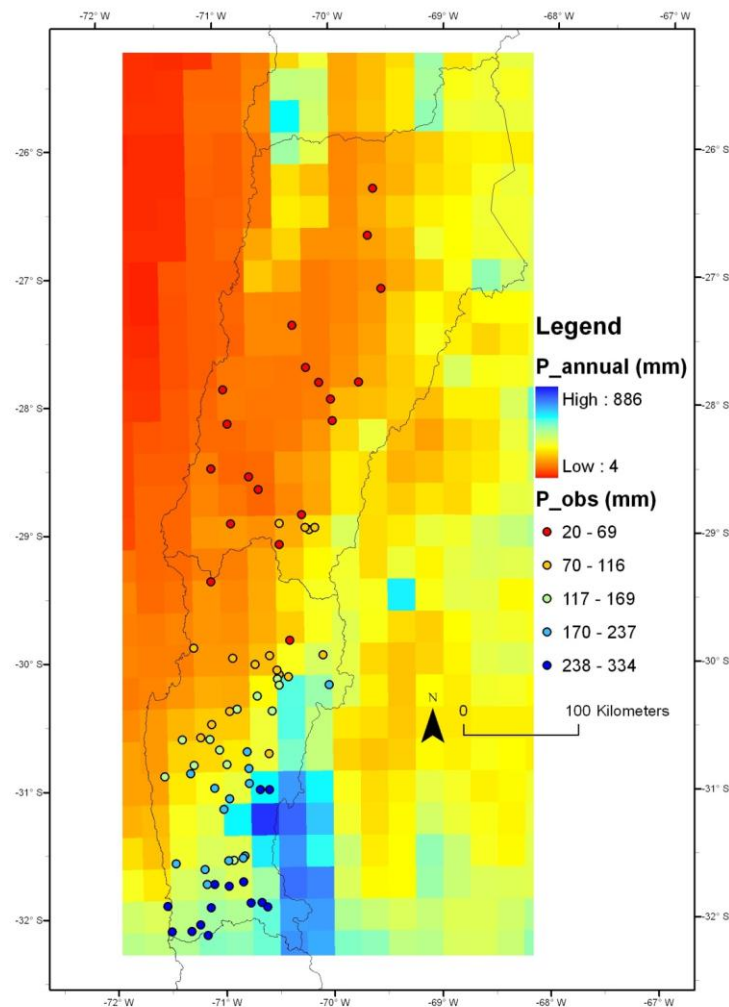


Figure 20 – Mean Annual Precipitation from TRMM (1998 – 2009)

By extracting values of the TRMM distribution at the observation points, we can compare the results of both models to the observations. On the Figure 21, we represent the mean annual precipitation over precipitation gauges calculated from observations and estimations. As the overlapping period between TRMM and the gauges dataset is limited to 9 years, we chose to compare the annual mean precipitation calculated over 1975-2006 with the annual mean TRMM prediction over 1998-2009, assuming a stationary distribution of the annual precipitation.

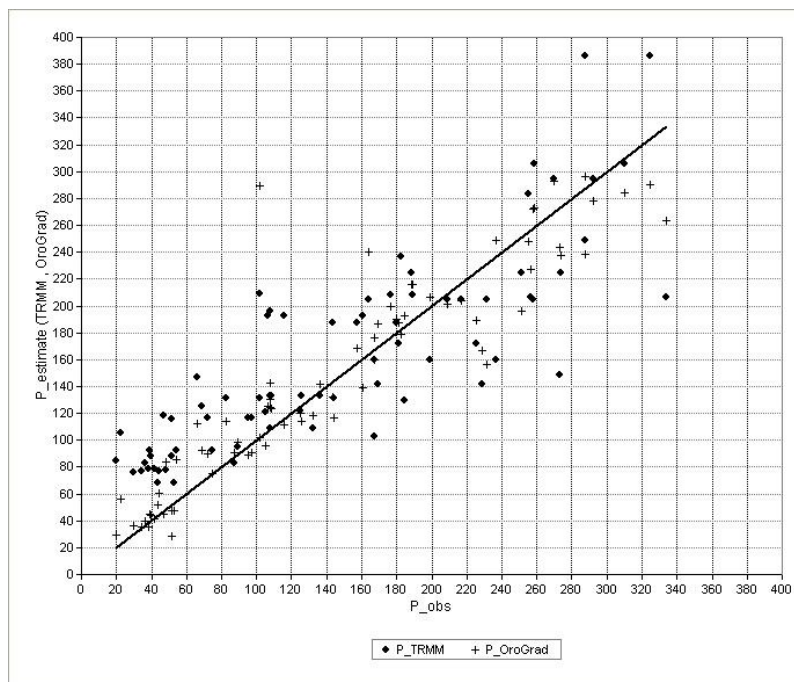


Figure 21 – Comparison of mean annual precipitation – Observations and estimations from TRMM (black circle) and orographic correction factor method (cross).

The estimations from TRMM are less correlated with observations than the estimations from our model. The strong precipitation gradient with latitude is not reproduced as well. TRMM underestimates the high precipitations and overestimates the low precipitations.

The monthly amounts of precipitation from TRMM were also tested the same way as the estimations of the orographic correction factor model. For this comparison, we limit the period of calculation to the overlapping period 1998-2006. This time, the performances of the model TRMM are much lower (Figure 22) (Table 6).

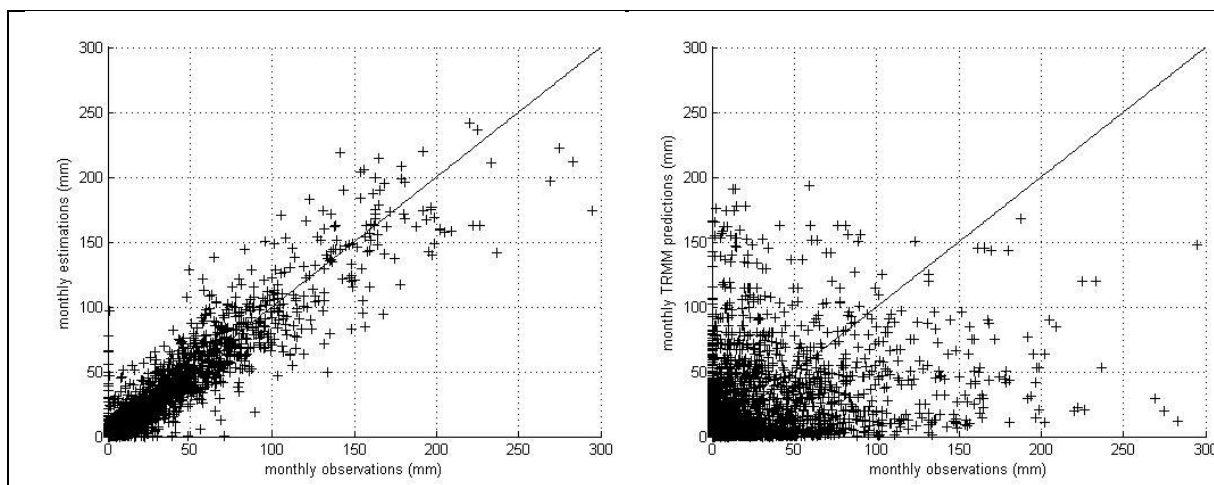


Figure 22 - Scatter plot of monthly precipitation (simulations versus observations). Comparison between the estimations calculated with the model of orographic correction factor (left) and the TRMM predictions(right). The period of calculation is the overlapping period 1998-2006.

Efficiency	Orographic correction	TRMM
NSE	0,80	-1,39
KGE	0,76	-0,19
Biais (%)	1,05	1,66
Mean Relative Bias (%)	17,36	65,11

Table 6 - Test of monthly estimations of TRMM

At this first step of validation, the interpolation model of orographic correction factor appears thus better than TRMM but not really better than a widely used interpolation model like IDW.

#### 4.3.2. Brief qualitative analysis of results from previous studies

The comparison between our estimations and what can be found in previous studies like [Souvignet, 2007] or [Morales et al., 2004] allows a first qualitative test of this work. In high altitude areas, our estimations are in general lower than those proposed by Souvignet [2007]. The difference in period of calculation cannot explain by itself these discrepancies. On the contrary, our estimations are higher than those provided by Morales and al. [2004]

Favier and al. [2009] reports the estimation of Ginot and al. [2006] about the mean annual precipitation at glacier Tapado (Elqui valley) de  $315 \text{ mm.a}^{-1}$  based on the interpolation from the precipitation gauges located downstream. Our estimation is here around  $300 \text{ mm.y}^{-1}$ .

In conclusion of this first test, our estimations in high-altitude areas are set in the range of what was provided by different authors in previous studies. The next part will investigate more meticulously the estimations by comparing them to the sparse observations available that consist in seasonal snowpack measurements.

#### 4.3.3. Determining the period of solid precipitation

The comparison between estimations and snow water equivalent measurements is pertinent if only if the solid part of the precipitation is taken into account. As we described previously, the snowfalls occur in winter and the snowpack is present between May and September to October (Figure 2). For example, a 24-years long record at the mining site of El Indio (Table 1) reveals that 81% of annual precipitation occurs as snow in winter (MJJA). We use thus the period May-October.

#### 4.3.4. Comparison between estimations and snow water equivalent measurements

##### 4.3.4.1. Daily SWE measurements

We consider first the set of daily SWE measurements (Table 7). The Figure 23 shows the comparison of annual amounts of solid precipitations derived from the observations and different models of estimation. We focus on three models : the model of orographic correction factor, the IDW model, and the TRMM model.

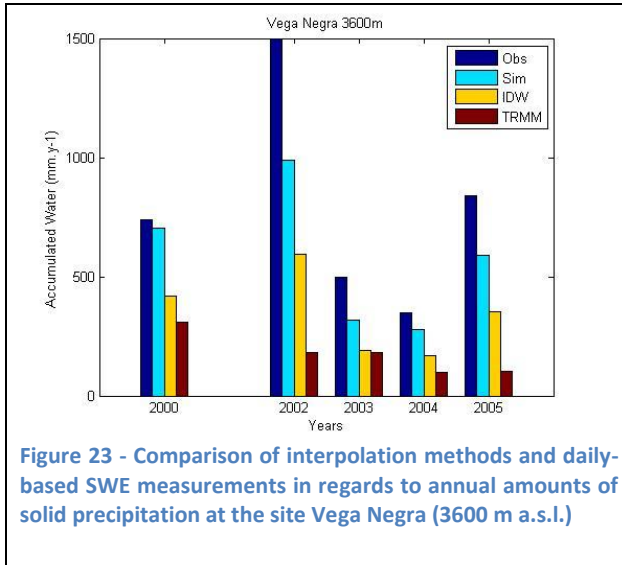


Figure 23 - Comparison of interpolation methods and daily-based SWE measurements in regards to annual amounts of solid precipitation at the site Vega Negra (3600 m a.s.l.)

	Vega_Negra	Q_Larga	Soledado
N years	5	4	2
Obs (mm/y)	786	550	425
Sim (mm/y)	576	440	382
IDW (mm/y)	346	261	235
TRMM (mm/y)	175	343	432

Table 7 - Results of mean annual snow accumulation. Observations are here provided by daily SWE measurements

This first result seems to underline the best capacity of our model to predict the winter snow accumulation in high-altitude watersheds. Yet, the conclusions should be taken careful because of the lack of available data. The IDW and TRMM method tend to underestimate the winter precipitation.

The Figure 24 displays the results of the interpolation methods. The best simulation is achieved with the method of orographic correction factor. The scarcity of this data make a further analysis difficult. In particular, we do not test the monthly predictions.

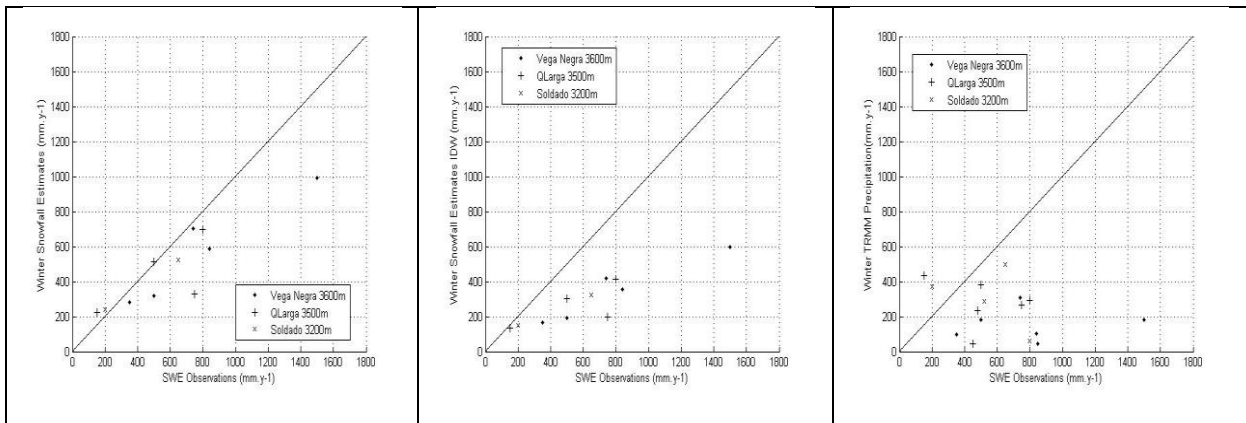


Figure 24 - Comparison of different methods of estimation (from left to right : orographic correction factor method, IDW and TRMM). The estimations of yearly snow accumulation at the three sites where daily snow water equivalent are here plotted with the observations.

#### 4.3.4.2. Monthly and variable SWE measurements

Given the difficulties noticed about the SWE measurements, the comparison between the mean annual precipitation observed and simulated with the orographic correction factor method is quite promising. The analysis of the annual amounts of snow accumulated reveals however that this result is partly explained by annual underestimated amounts compensating overestimated ones. Yet, the method of orographic correction factor provides better results than other ones we tested: IDW and TRMM. The comparative results of yearly annual precipitation at the SWE sites are presented in Table 8 and Table 9.

Id_Snow	Name	Source	Lon	Lat	Alt (m)	SWE_Obs (mm/y)	Years	P_Obs (mm/y)	P_Oro.Corr. (mm/y)	P_IDW (mm/y)	P_TRMM (mm/y)
1	El Indio	Mining Cie	-69,97	-29,75	3869	172	24	172	177	114	134
2	Pascua-Lama	Mining Cie	-70,07	-29,27	3717	174	6	179	118	67	123
3	Vega Negra	DGA	-70,52	-30,92	3600	538	25	538	492	296	168
4	Quebrada Larga	DGA	-70,37	-30,72	3500	328	19	328	371	222	286
5	Soldado	DGA	-70,33	-32,00	3200	456	23	456	420	258	330
6	Olivares	DGA	-69,95	-30,25	3550	149	23	149	182	166	49
7	Sobrante	DGA	-70,47	-32,18	3250	437	20	437	455	267	330

**Table 8 - SWE measurements sites and mean annual snow accumulation. P\_obs, P\_oro.corr et P\_IDW are mean annual calculated over the same period, i.e the years within the period 1975-2006 where observations are available. On the contrary, P\_TRMM is calculated over the period 1998-2009.**

The Figure 25 shows the comparison between snowfall estimations from the study method and available observations. The performance of the different models is quantified by two criterions (Table 9). For the correlation coefficient, the data are aggregated to a unique vector of observations and a unique vector of estimations (one for each model in fact). The relative bias of mean annual solid precipitation is calculated separately for each site.

			Orographic Correction	IDW	TRMM
R <sup>2</sup>			<b>0,7929</b>	<b>0,7633</b>	<b>0,0529</b>
Id_Snow	Name	Alt (m)	Relative Bias (%)		
1	El Indio	3869	3,2	-33,5	-22
2	Pascua-Lama	3717	-34,0	-62,7	-31,3
3	Vega Negra	3600	-8,5	-44,9	-68,9
4	Quebrada Larga	3500	13,3	-32,4	-12,9
5	Soldado	3200	-7,9	-43,3	-27,5
6	Olivares	3550	22,1	11,1	-67,1
7	Sobrante	3250	4,0	-39,0	-24,4

**Table 9 – Evaluation of models predictions and comparison between models performance**

Considering the orographic correction factor model, there is no trend to under or overestimation. The annual variability is reproduced and the mean annual snow accumulation is close to the observed one. The IDW model has the same behaviour as the first one but tends to systematically underestimate the precipitation. This highlights the effect of the orographic correction in the first case and this correction improves the prediction at the observation site.

Finally, the TRMM estimations reproduce partly the annual variability but the biases on the annual amounts are important. The spatial variability is also difficult to assess due to the low resolution. Thus, the TRMM estimations are equal for the sites Soldado and Sobrante (distance = 24 km).

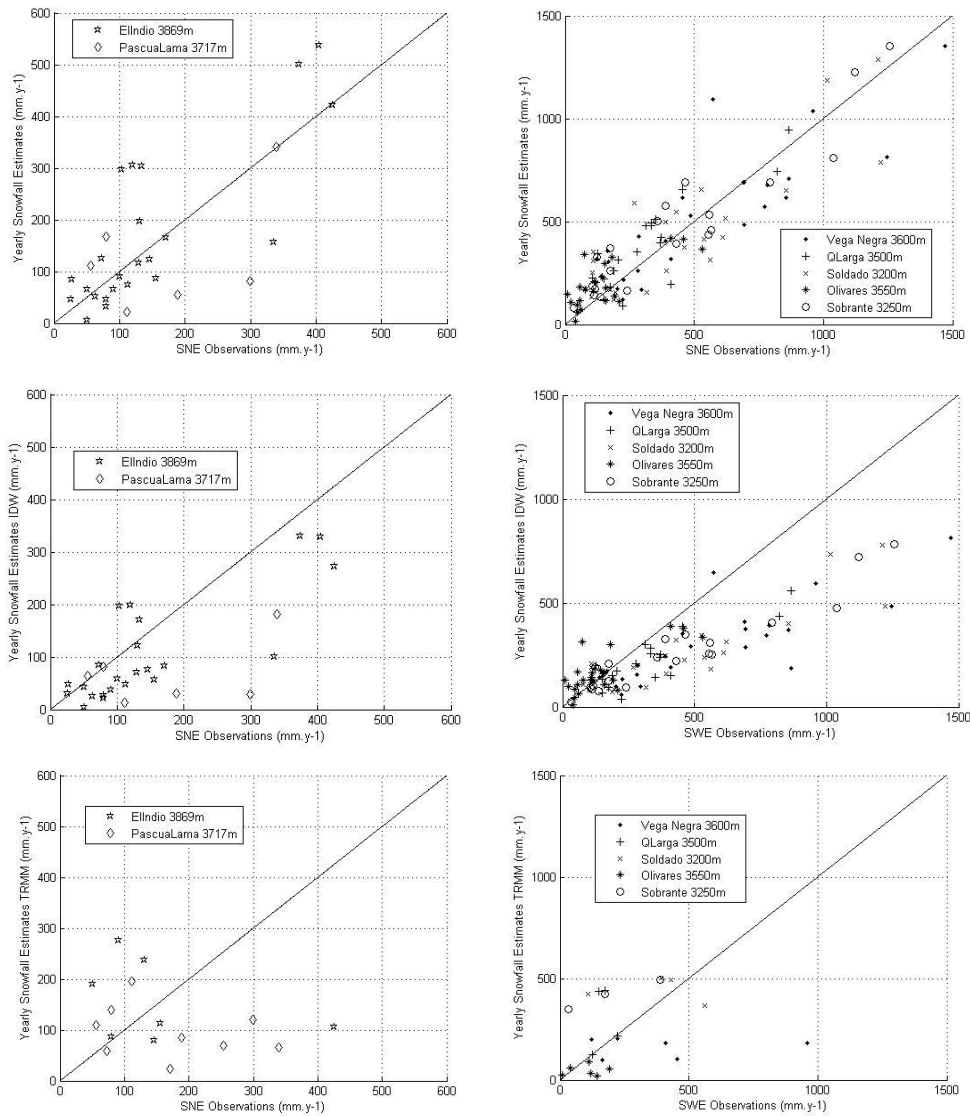


**Figure 25 - Scatter plot of snow fall estimations (respectively Orographic Correction Method, IDW and TRMM) versus Snow Water Equivalent Measurements. We separate data in two sets : data provided by mining companies (i), the yearly SWE is here derived from monthly observations and data from DGA (ii), the SWE is taken as the maximum of snow accumulation recorded by snow courses (maximum three records per year).**

In conclusion of this section, in spite of the lack of observation data in high-altitude areas of the Norte Chico region, the consideration of available snow water equivalent measurements enables to validate the effect of orographic correction in our model, which was not evident in the cross-validation process. We can conclude that the correction factor improves the accuracy of winter precipitation predictions. Moreover, our model appears better than the TRMM outputs.

## 4.4. Third level of validation: Runoff coefficients and water balance

### 4.4.1. Runoff coefficients

Following what had been suggested by Favier and al. [2009], the runoff coefficients are calculated for each catchments and upstream subcatchments. We calculate the ratio of the mean annual runoff on the mean annual precipitation for each watershed. In spite of his simplicity, this first test is an easy and efficient way to compare the influence of different spatial distribution of precipitation on the physical reality of the water balance. The mean discharge is computed over the same period as the mean annual precipitation. The annual mean areal precipitation is obtained by spatial integration using the GIS software (intersection of the interpolation grid cells with each of the polygon representing the catchments). The results are displayed in the Figure 26 below.

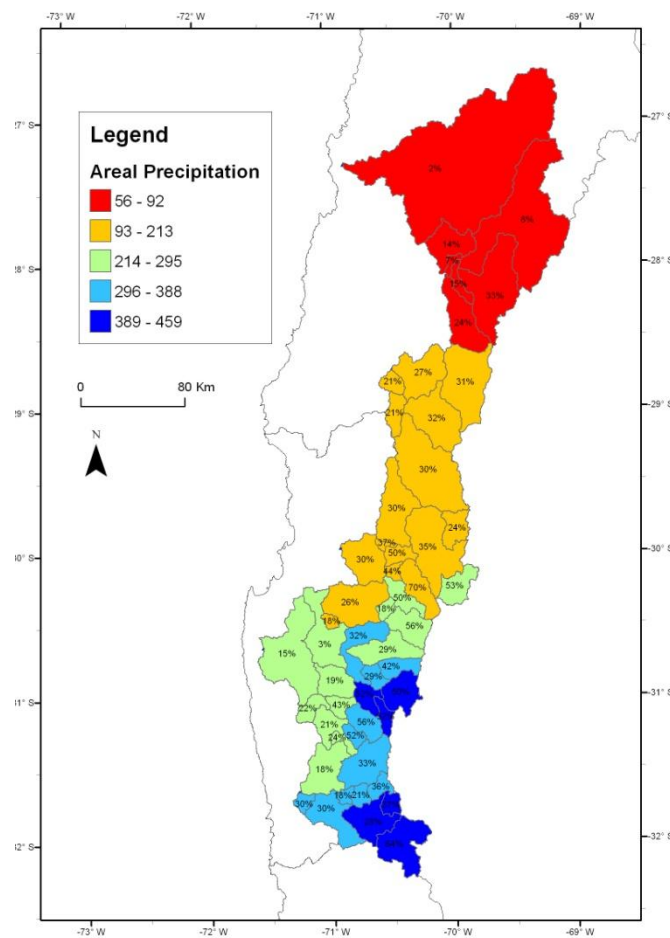


Figure 26 – Annual mean areal precipitation and runoff coefficients over the Norte Chico watersheds.

The runoff coefficients over all subcatchments are less than 100%, which is the physical limit of the water balance. Furthermore, runoff coefficients increase strongly with altitude. This is consistent with the fact that downstream catchments are more affected by water losses due to both natural (evapotranspiration) and human factors (irrigation).

We compare the results to other calculations using different spatial precipitation distribution.

#### 4.4.1.1. Simple interpolation scheme [Favier et al., 2009]

To compute the runoff coefficients, Favier and al. [2009] first used the simple interpolation scheme we described previously in order to obtain watershed precipitations. The coefficients they obtained are bigger than 100% in several of the upper catchments (which led them to entitle their paper “Interpreting discrepancies between discharge and precipitation in high-altitude area of Chile’s Norte Chico region”). For all the watersheds but one, the runoff coefficient obtained by the method of orographic correction factor is lower than the one calculated by Favier and al. [2009](Figure 27). This comes from highest watershed precipitation estimations, up to two times the estimations of Favier and al. [2009].

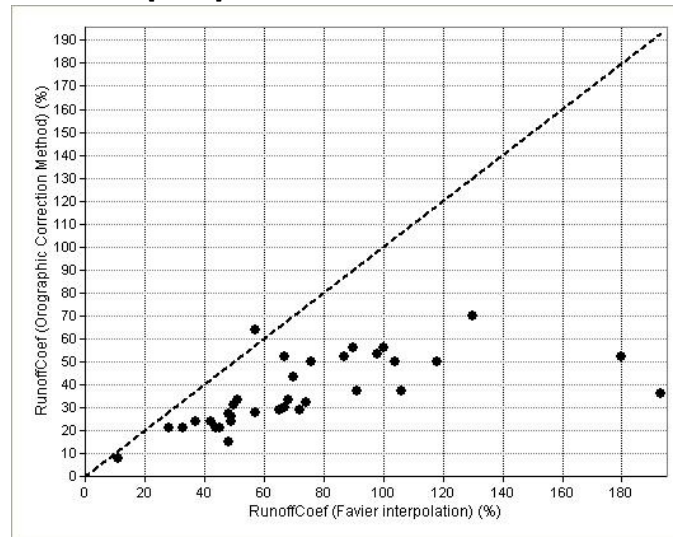


Figure 27 – Comparison between runoff coefficients calculated using the method of orographic correction factor and the runoff coefficients reported by Favier and al. [2009] using a simple interpolation scheme.

#### 4.4.1.2. Consideration of atmospheric prediction model [Favier et al., 2009]

Due to the large discrepancies between precipitation and discharge, Favier and al. [2009] suggested to consider spatial distribution of precipitation derived from global forecast system atmospheric prediction model to calculate watershed precipitation. The mean annual areal precipitation is enhanced for the majority of catchments with a factor between 1 and 2. The water budget is improved in 8 of the 12 high-altitude catchments but some are still too large (>100 %, runoff excess).

#### 4.4.1.3. TRMM

The consideration of TRMM did not improve the accuracy of precipitation predictions in high-altitude areas (section 4.3.4.2). Yet, the good performances of TRMM considering the predictions of mean annual precipitation over the precipitation gauges (section 4.3.1) incite us to compare it with our model in regards to runoff coefficients calculations (Figure 28). In general, the mean areal precipitation derivated from the TRMM estimation is similar to the one derivated from the orographic correction factor model and so is the runoff coefficient.

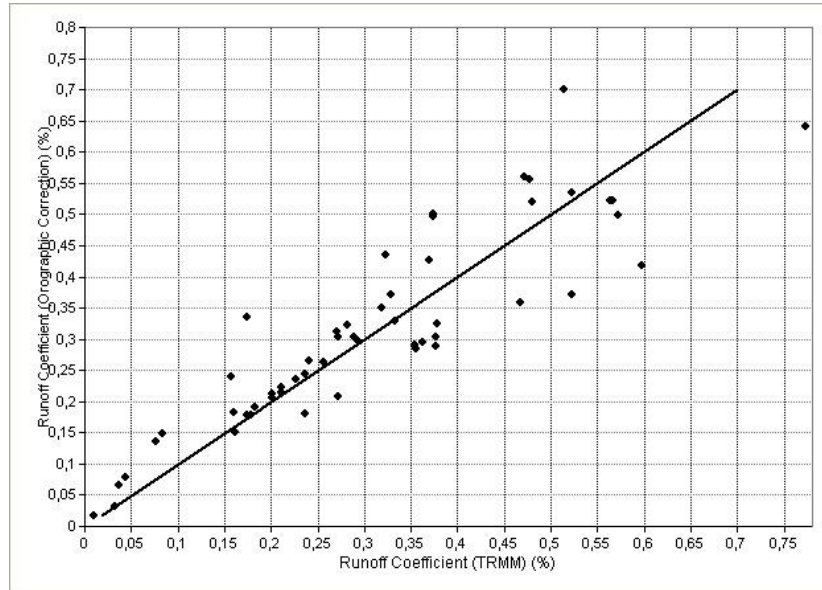


Figure 28 - Comparison between runoff coefficients calculated using the method of orographic correction and the satellite project TRMM.

#### 4.4.2. Water balance calculation

##### 4.4.2.1. Method – Simplified water balance

We aim to further evaluate the spatial interpolation of precipitation by closing the water balance equation for various catchments. The following water balance equation was used :

$$Q = P - E \quad (\text{Equation 8})$$

Where Q is the mean annual discharge, P the mean annual areal precipitation and E the mean annual water losses.

Due to the semi-arid and mountainous characteristics of the study region, the estimation of evapotranspiration is very difficult. According to Favier and al. [2009], evaporation from soil and transpiration are assumed to be negligible because, above 3000 m a.s.l, the catchments are steep, rock covered, and vegetation is totally absent except in the close vicinity of rivers. Simulation results with the atmospheric prediction model WRF also suggest that evaporation is absent without snow cover [Favier et al., 2009] (see also pictures in the section description of Norte Chico). This incite us to focus on high-altitude watersheds where moreover discharge is less affected by water extraction for irrigation. We assume that water losses are limited to sublimation from snow cover areas. The other terms of the water budget calculation are neglected. Due to the small extent of the glaciers in the region (1 to 2 % of the total surface area for the most glacierized catchment : la Laguna Embalse), the term of change in long-term storage is set to zero. The groundwater interannual storage is also neglected. This hypothesis is rational in the upstream watersheds where aquifers only occur in narrow valleys bottoms. It is less reliable in the downstream subcatchments.

##### 4.4.2.2. Water losses from snow cover surface - Estimation of mean sublimation

We aim to estimate for each catchment a mean annual volume of water losses due to sublimation. We calculate first the mean annual snow cover area (SCA) for each catchment and then apply a mean daily sublimation rate. The snow cover area is derived from MODIS imagery (Figure 29).

We searched for estimations of daily sublimation rate in the scientific literature. Ginot and al. [2006] suggest a mean annual sublimation of  $327 \text{ mm.y}^{-1}$  on Cerro Tapado glacier (Elqui valley) for the 1962-1999 period. This estimation was derived from interpretation of deep ice core measurement. The ratio sublimation/ablation (R) is 89% (11% melt).

The sublimation measurements at Pascual-Lama made by the CEAZA using snow lysimeters were also considered (Figure 30 and Figure 31). The mean ratio sublimation/ablation is 77%. In equation 8, the term E of water loses is calculated as a fraction of precipitation P. As we assumed that there is no interannual water storage (the whole annual snowpack has disappeared at the end of the melt season), the annual ablation is equal to the annual snowfall. The term E is thus calculated as follows:

$$E = R \times SCA \times P \quad (\text{Equation 9})$$

And the water balance equation can be written as follows:

$$Q = P \times (1 - (R \times SCA)) \quad (\text{Equation 10})$$

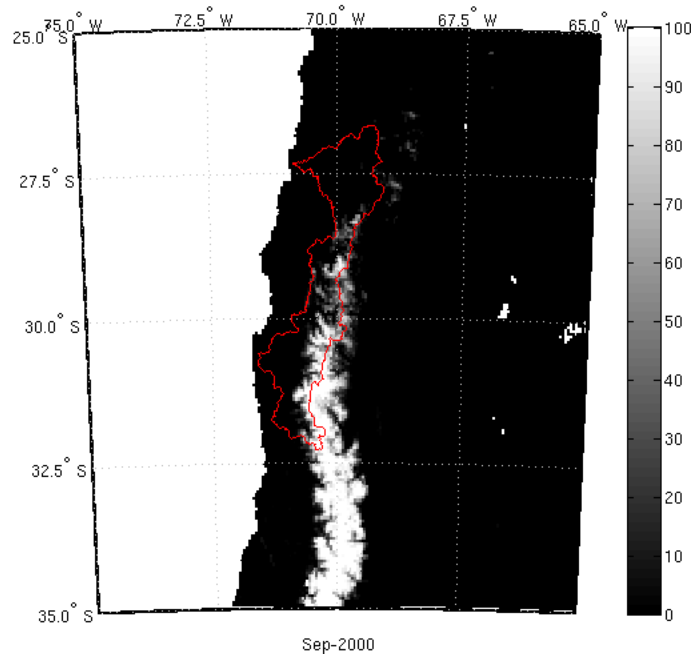


Figure 29 - Example of estimation of Snow Cover Area. The red line delimits the studied watersheds.

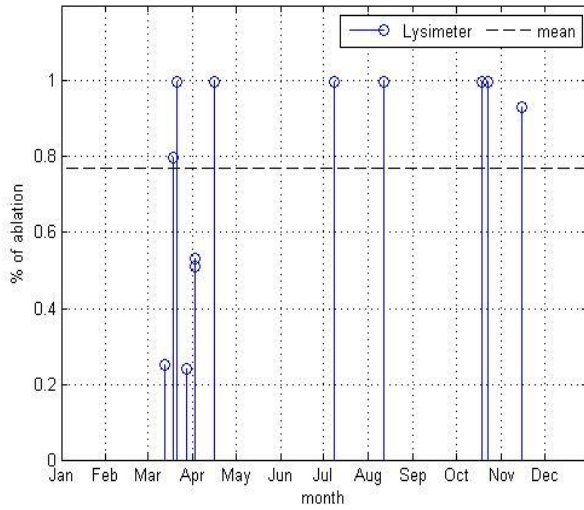


Figure 30 –Lysimeter experiments results in Pascua-Lama : fraction of sublimation in snow ablation



Figure 31 - Example of snow lysimeter measurement at the site Pascua-Lama (CEAZA)

The results of water balance calculations are displayed in Figure 32.

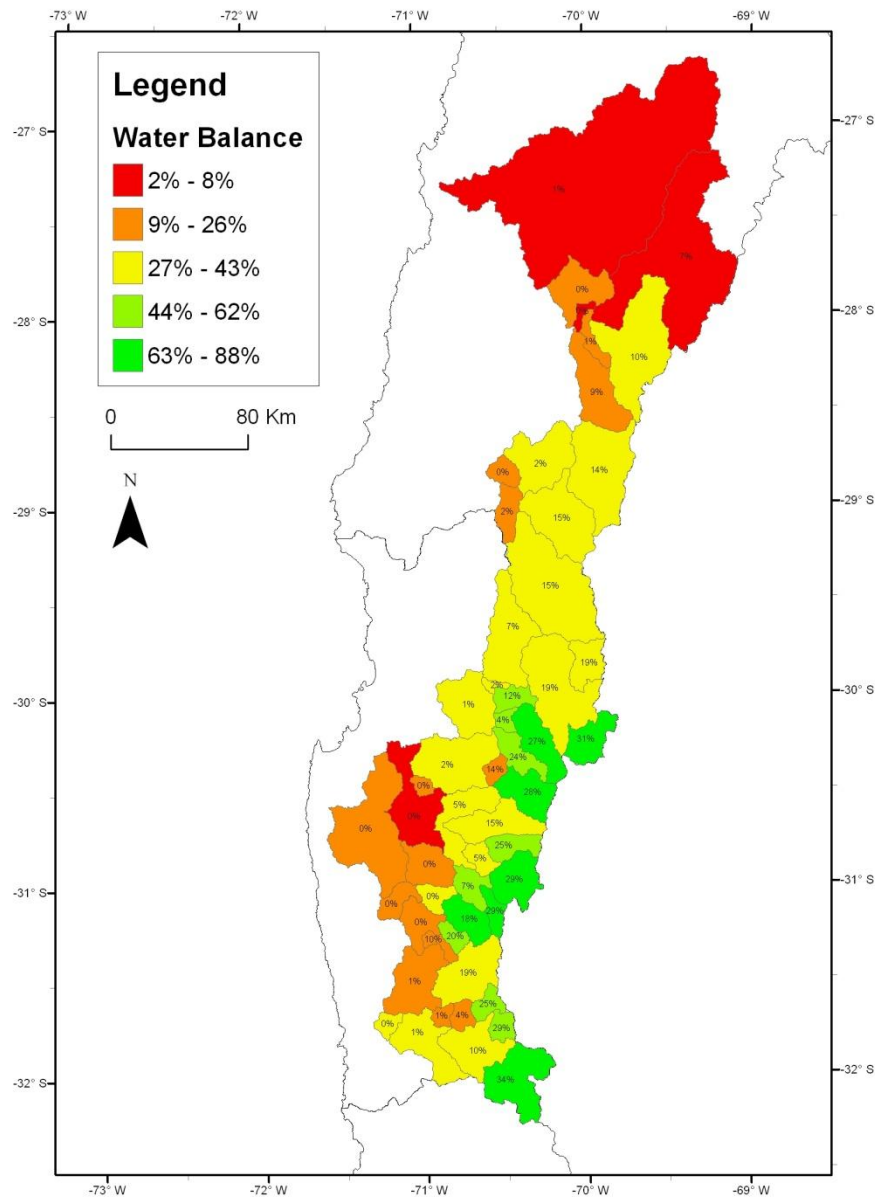


Figure 32 - Snow Cover Area (text labels) and water budget calculation. The terms of the equation are all annual means. Here R is set to 0,77 (measurements from CEAZA)

The range of SCA is 0-34%. The largest values are found in the highest subcatchments. For all the high-altitude catchments, the ratio ( $Q^{obs} / P^{sim} - E$ ) becomes closer to 100% without exceeding this physical limit. The low values calculated for most of the subcatchments downstream may be explained by water losses more important than in altitude (evaporation, infiltration and irrigation). At least one high-altitude catchment in the northern part of the region have a runoff deficit very high. The water losses by sublimation may be underestimated in this area of extreme solar radiation. Moreover, the variability of precipitation between the coastal areas and the altitude areas is particularly strong at this latitude and the uncertainty about the precipitation interpolation is high.

The introduction of our rough estimation of sublimation improve the water balance. As a result, we can conclude that the precipitation input is realistic and is a first step towards a better representation of the water balance in the high-altitude areas of Norte Chico.

## 5. Error assessment

Finally, we propose a short and empirical analysis of the error range associated with the method of orographic correction factor. The set of precipitation gauges is sorted by the mean annual precipitation estimation and then separated in three parts containing 25 precipitation gauges each one. The empirical limits of the 70%-error confidence intervals are calculated. For each part, the confidence interval contains thus 17 precipitation gauges. The error range decreases with the precipitation estimation. Thus, the relative bias  $P^{\text{sim}}/P^{\text{obs}}$  is larger for the precipitation gauges with small amounts of precipitation than for the ones located in dryer areas. By extrapolation, we assume that given an estimated precipitation, the relative bias associated can be assessed (Figure 33). More work is needed to include these errors in the three levels of validation.

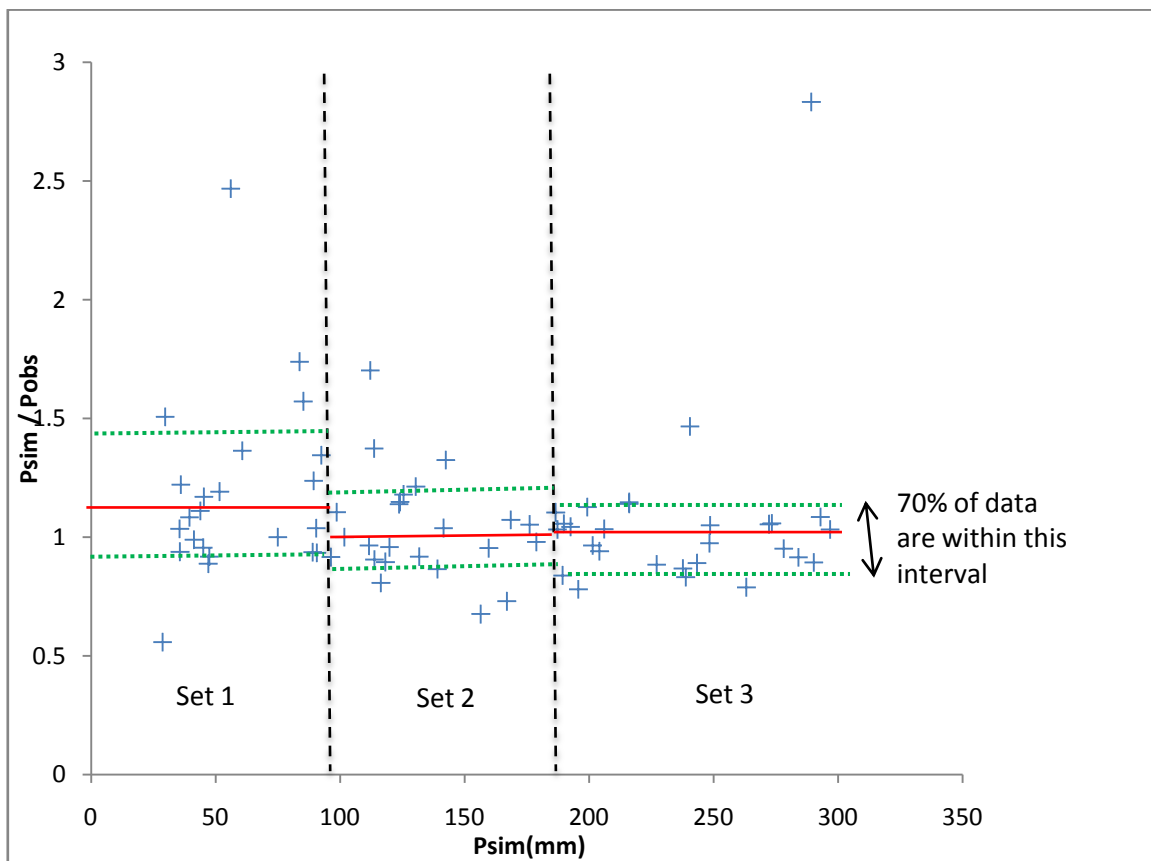


Figure 33 - Empirical method for error assessment. The data set is the precipitation observations and estimations over the gauges. The red line represents the mean for each set and the the interval in green dashed line is the 70% error confidence interval.

## Conclusions

Our goal was to improve the water balance of high-altitude watersheds in the Norte Chico region. Despite the importance of water resources for this semi-arid region in development and the high dependence in regards to snow melt water from the Cordillera, the hydrological processes in high-altitude still are poorly known and remain difficult to assess. We focused in this work on the spatial interpolation of precipitation over the entire region. The strong variability of precipitation and the lack of data in altitude were the main difficulties we faced. In comparison to other methods of precipitation interpolation, the interpolation method proposed by Valery [2009] gave better results at three different levels of validation. In particular, the runoff coefficients in high-altitude catchments calculated with this spatial distribution of precipitation are more realistic than those obtained by Favier and al. [2009]. Yet, the evaluation of the water balance accuracy is limited by the possible biases of runoff measurements and the difficulties to assess the water losses. It is regardless a valuable method to better represent the high altitude water balance in the Norte Chico. As such, this work may provide a sound basis to future work where the knowledge of precipitation would be needed like for example further hydrological studies and works about the possible impacts of climate change.

In a context of global warming, the snow-dominated regions are particularly exposed to significant changes about water availability [Messerli *et al.*, 2004]. The consequences of the predicted warming over the hydrology and so the water availability in the regions are likely to be severe [Barnett *et al.*, 2005]. The successive reports of the Intergovernmental Panel for Climate Change (IPCC) make the concern about water availability in mountainous areas extend more than ever and mountain-dominated regions from all over the world are expected to be affected by the global warming with consequences about a large range of socio-economical items [Barnett *et al.*, 2005] [Vicuna *et al.*, 2010b]. In Norte Chico, recent studies about climate change impacts on water availability underline the rising concerns about future sustainability of a local economy largely dependent on irrigated agriculture, mining and increasing tourism activity, all of three requiring large amounts of fresh water [Souvignet, 2007] [Vicuna *et al.*, 2010a]. The need of estimation and modeling of water resources in Norte Chico in a global warming context is strengthened by the climate variability observed over the 20<sup>th</sup> century, that is, decreasing precipitation [Vuille and Milana, 2007] and aridification [Squeo *et al.*, 2007].

## Bibliography

- Barnett, T. P., J. C. Adam, and D. P. Lettenmaier (2005), Potential impacts of a warming climate on water availability in snow-dominated regions, *Nature*, 438(7066), 303-309.
- Barry, R. G. (Ed.) (2008), *Mountain weather and climate. 3rd edition*, 506 pp., Cambridge University Press.
- Benichou, P., and O. Le Breton (1987), Use of topography on mapping of statistical rainfall fields., *La meteorologie*, 19, 23-34.
- Buytaert, W., R. Celleri, P. Willems, B. De Bievre, and G. Wyseure (2006), Spatial and temporal rainfall variability in mountainous areas: A case study from the south Ecuadorian Andes, *J Hydrol*, 329(3-4), 413-421.
- Clark, M. P., and A. G. Slater (2006), Probabilistic quantitative precipitation estimation in complex terrain, *J Hydrometeorol*, 7(1), 3-22.
- Favier, V., M. Falvey, A. Rabatel, E. Praderio, and D. Lopez (2009), Interpreting discrepancies between discharge and precipitation in high-altitude area of Chile's Norte Chico region (26-32 degrees S), *Water Resour Res*, 45, -.
- Garreaud, R. D. (2009), The Andes climate and weather, *Advances in Geosciences*, 7, 1-9.
- Ginot, P., C. Kull, U. Schotterer, M. Schwikowski, and H. W. Gaggeler (2006), Glacier mass balance reconstruction by sublimation induced enrichment of chemical species on Cerro Tapado (Chilean Andes), *Clim Past*, 2(1), 21-30.
- Goovaerts, P. (2000), Geostatistical approaches for incorporating elevation into the spatial interpolation of rainfall, *J Hydrol*, 228(1-2), 113-129.
- Gottardi, F. (2009), Estimation statistique et reanalyse des precipitations en montagne - Utilisation d'ebauches par type de temps et assimilations des donnees d'enneigement - Applications aux grands massifs montagneux francais., These de Doctorat thesis, 261 pp, INPG Grenoble.
- Gupta, H. V., H. Kling, K. K. Yilmaz, and G. F. Martinez (2009), Decomposition of the mean squared error and NSE performance criteria: Implications for improving hydrological modelling, *J Hydrol*, 377(1-2), 80-91.
- Klemes, V. (1990), The modelling of mountain hydrology: the ultimate challenge, *IAHS-AISH Publication*, 190, 29-43.
- Messerli, B., D. Viviroli, and R. Weingartner (2004), Mountains of the world: Vulnerable Water Towers for the 21(st) century, *Ambio*, 29-34.
- Morales, L., F. Canessa, C. Mattar, and R. Orrego (2004), Comparison of stochastic and regression geostatistics interpolation methods for detection of microclimatic areas, edited.
- Ranzi, R. (2009), Are 2000m a.s.l. a last frontier in hydrology?, *Geophysical Research Abstracts*, 11.
- Souvignet, M. (2007), Climate Change Impacts on Water Availability in the Semiarid Elqui Valley, Chile.
- Squeo, F. A., M. Holmgren, M. Jimenez, L. Alban, J. Reyes, and J. R. Gutierrez (2007), Tree establishment along an ENSO experimental gradient in the Atacama desert, *J Veg Sci*, 18(2), 195-202.
- Valery, A., V. Andreassian, and C. Perrin (2009a), What do we know about precipitation orographic gradients in mountainous areas? A comparative analysis in Canada, France, Sweden and Switzerland, *Geophysical Research Abstracts*, 11, 12725-12725.
- Valery, A., V. Andreassian, and C. Perrin (2009b), Inverting the hydrological cycle: when streamflow measurements help assess altitudinal precipitation gradients in mountain areas, *IAHS Publ.*, 333.
- Valéry, A. (2009), Thèse de Doctorat, Modélisation précipitations-débit sous influence nivale. Elaboration d'un module neige et évaluation sur 380 bassins versants.
- Vicuna, S., R. Garreaud, and J. Mc Phee (2010a), Climate change impacts on the hydrology of a snowmelt driven bassin in semiarid Chile, *Climatic Change*.
- Vicuna, S., J. A. Dracup, J. R. Lund, L. L. Dale, and E. P. Maurer (2010b), Basin-scale water system operations with uncertain future climate conditions: Methodology and case studies, *Water Resour Res*, 46, -.
- Viviroli, D., and R. Weingartner (2004), The hydrological significance of mountains: from regional to global scale, *Hydrol Earth Syst Sc*, 8(6), 1016-1029.
- Vuille, M., and J. P. Milana (2007), High-latitude forcing of regional aridification along the subtropical west coast of South America, *Geophys Res Lett*, 34(23), -.
- Weingartner, R., D. Viviroli, and B. Schadler (2007), Water resources in mountain regions: a methodological approach to assess the water balance in a highland-lowland-system, *Hydrol Process*, 21(5), 578-585.

## Figures

Figure 1 - Location of the region Norte Chico.....	7
Figure 2 - Mean seasonal snow cover area derived from MODIS satellite imagery.....	8
Figure 3 – (a) - Annual Precipitation at La Serena (Id 32 – see Figure 1) between 1975 and 2005. (b)- Seasonal variation of precipitation and discharge in Norte Chico region. The open bars are mean monthly precipitation between 1900 and 2005 at La Serena (Id 32 – table of precipitation gauges in annex and Figure 1 above). The continuous line is mean monthly discharge at La Laguna Embalse (Id 11 – see table of runoff stations in annex) between 1964 and 2005. The dashed line is mean monthly discharge of Hurtado River at Recoleta Dam (Id 24) between 1928 and 1984 (from [Favier et al., 2009]). .....	9
Figure 4 extracted from [Souvignet, 2007] – Isohyets for the Elqui Watershed after data provided by the DGA and CEAZA .....	11
Figure 5 extracted from [Favier et al., 2009] - Example of the methodology used to estimate catchment scale precipitation .....	11
Figure 6 – Spatial distribution of precipitation over Coquimbo region computed by multiple regression, from [Morales et al., 2004] .....	12
Figure 7 - Localization of available snow water equivalent measurement sites .....	15
Figure 8 - Example of daily snow water equivalent measurements provided by DGA. Here is plotted the snow accumulation in Quebrada Larga (see table below to localisation) in the year 2008. In our analysis, the intermediate melts have been taken in count. The SWE is thus taken as the maximum of the vertical line plus the intermediate melts. ....	16
Figure 9 - seasonal model for NSE efficiency.....	18
Figure 10 – Efficiency of different sets of parameters in cross-validation. The figure above represents the NSE efficiency while the figure below represents the KGE efficiency.....	20
Figure 11 - Performances at precipitation gauges in cross-validation .....	21
Figure 12 - Seasonal distribution of orographic correction factors .....	22
Figure 13 – Relationship between annual optimized orographic correction factor and ENSO.....	23
Figure 14 – Scatter plots of monthly precipitation observations (bottom axis) and estimations (left axis) at Pisco Elqui (Id 25 – Elqui Valley) and Lautaro (Id 62 – Copiapo Valley). ....	24
Figure 15 – Mean annual precipitation observation $P^{obs}$ at precipitation gauges.....	24
Figure 16 - Spatial distribution of relative bias and scatter plot of mean annual precipitation observation (bottom axis) and estimations (left axis). The color of circles refer to the relative bias. ....	25
Figure 17 - Different scenarios of parametrization.....	26
Figure 18 – Relative Bias vs Altitude for scenarios 2 (triangles) and 3 (circles).....	27
Figure 19 - Spatial distribution of mean annual precipitation computed with orographic correction factor method and mean annual precipitation observed at precipitation gauges .....	29
Figure 20 – Mean Annual Precipitation from TRMM (1998 – 2009) .....	30
Figure 21 – Comparison of mean annual precipitation – Observations and estimations from TRMM (black circle) and orographic correction factor method (cross). ....	31
Figure 22 - Scatter plot of monthly precipitation (simulations versus observations). Comparison between the estimations calculated with the model of orographic correction factor (left) and the TRMM predictions(right). The period of calculation is the overlapping period 1998-2006. ....	31
Figure 23 - Comparison of interpolation methods and daily-based SWE measurements in regards to annual amounts of solid precipitation at the site Vega Negra (3600 m a.s.l.) .....	33

Figure 24 - Comparison of different methods of estimation (from left to right : orographic correction factor method, IDW and TRMM). The estimations of yearly snow accumulation at the three sites where daily snow water equivalent are here plotted with the observations. ....	33
Figure 25 - Scatter plot of snow fall estimations (respectively Orographic Correction Method, IDW and TRMM) versus Snow Water Equivalent Measurements. We separate data in two sets : data provided by mining companies (i), the yearly SWE is here derived from monthly observations and data from DGA (ii), the SWE is taken as the maximum of snow accumulation recorded by snow courses (maximum three records per year). ....	35
Figure 26 – Annual mean areal precipitation and runoff coefficients over the Norte Chico watersheds. ....	36
Figure 27 – Comparison between runoff coefficients calculated using the method of orographic correction factor and the runoff coefficients reported by Favier and al. [2009] using a simple interpolation scheme. ....	37
Figure 28 - Comparison between runoff coefficients calculated using the method of orographic correction and the satellite project TRMM. ....	38
Figure 29 - Example of estimation of Snow Cover Area. The red line delimits the studied watersheds. ....	39
Figure 30 –Lysimeter experiments results in Pascua-Lama : fraction of sublimation in snow ablation ....	40
Figure 31 - Example of snow lysimeter measurement at the site Pascua-Lama (CEAZA).....	40
Figure 32 - Snow Cover Area (text labels) and water budget calculation. The terms of the equation are all annual means. Here R is set to 0,77 (measurements from CEAZA) .....	41
Figure 33 - Empirical method for error assessment. The data set is the precipitation observations and estimations over the gauges. The red line represents the mean for each set and the the interval in green dashed line is the 70% error confidence interval. ....	42

### Tables

Table 1 - Snow Water Equivalent (SWE).....	15
Table 2- Optimized orographic correction factor for each watershed.....	21
Table 3 - Efficiency of seasonal distribution of orographic correction factors.....	22
Table 4 - Comparaision of three scenarios of parametrization .....	26
Table 5 - Scenarios 2 and 3 at la Laguna Embalse (Id 21 – 3100m a.s.l.).....	27
Table 6 - Test of monthly estimations of TRMM .....	32
Table 7 - Results of mean annual snow accumulation. Observations are here provided by daily SWE measurements.....	33
Table 8 - SWE measurements sites and mean annual snow accumulation. $P_{obs}$ , $P_{oro.corr}$ et $P_{IDW}$ are mean annual calculated over the same period, i.e the years within the period 1975-2006 where observations are available. On the contrary, $P_{TRMM}$ is calculated over the period 1998-2009.....	34
Table 9 – Evaluation of models predictions and comparison between models performance .....	34
Table 10 - Precipitation gauges .....	48
Table 11 - Runoff stations.....	48

## ANNEXES

Id	P_Stat	Lon	Lat	Alt	Pobs	P_est	P_TRMM	P_IDW	Pest_Err	Ptrmm_	
										Err	P_IDW_Err
		DD	DD	m	mm/y	mm/y	mm/y	mm/y	%	%	
1	LasBurras	-70,82	-31,53	1250	217	204	212	201	-5,94	-2,34	-8,22%
2	Cuncumen	-70,62	-31,93	1080	292	278	314	277	-4,87	7,41	-5,60%
3	SanAgustin	-70,83	-31,73	1050	258	272	215	272	5,45	-16,72	5,17%
4	LaTranquilla	-70,67	-31,90	975	270	293	314	292	8,46	16,29	7,52%
5	La Canela DMC	-70,92	-31,57	880	164	241	212	240	46,62	29,24	31,71%
6	Coiron	-70,77	-31,90	840	334	263	261	264	-21,12	-21,76	-26,41%
7	Huintil	-70,97	-31,57	650	232	157	212	157	-32,40	-8,45	-47,79%
8	Salamanca	-70,97	-31,77	510	257	227	215	229	-11,54	-16,28	-12,24%
9	MalPaso	-71,10	-31,75	375	251	196	243	194	-22,01	-3,16	-29,07%
10	Limahuida	-71,17	-31,75	295	188	216	243	215	14,75	29,06	12,48%
11	Illapal-DGA	-71,18	-31,63	290	177	199	243	198	12,69	37,40	10,83%
12	Mincha Norte	-71,45	-31,58	50	180	190	188	188	5,63	4,61	4,65%
13	LosVilosDMC	-71,53	-31,92	10	273	243	217	249	-10,89	-20,51	-9,82%
14	Culimo	-71,23	-32,07	580	259	273	270	273	5,76	4,44	5,20%
15	Quelon	-71,17	-32,15	960	310	284	295	281	-8,47	-4,95	-10,44%
16	LosCondores	-71,32	-32,12	260	255	248	247	249	-2,59	-3,12	-2,53%
17	Quilimari	-71,50	-32,12	25	287	239	247	240	-16,89	-14,02	-19,45%
18	Caimanes	-71,13	-31,93	395	274	238	270	238	-13,19	-1,39	-14,89%
19	SantaVirgina	-70,83	-31,55	980	209	201	212	200	-3,53	1,56	-4,23%
20	El Trapiche	-71,08	-29,38	300	48	84	91	82	73,95	88,98	41,32%
21	Laguna Embalse	-70,03	-30,20	3160	182	179	281	167	-2,00	54,02	-9,41%
22	Juntas	-70,08	-29,97	2155	107	142	224	143	32,54	108,41	24,76%
23	Rivadavia	-70,57	-29,97	850	105	96	122	103	-8,41	16,01	-2,49%
24	Huanta	-70,38	-29,85	1240	66	112	135	108	70,30	104,97	38,75%
25	Pisco Elqui DMC	-70,48	-30,12	1300	116	112	180	111	-3,55	55,57	-3,97%
26	Los Nichos	-70,50	-30,15	1350	144	116	321	116	-19,23	122,65	-24,39%
27	La Ortiga	-70,48	-30,20	1560	161	139	321	139	-13,42	99,83	-15,29%
28	Cochiguaz	-70,40	-30,13	1560	106	126	321	124	18,00	201,76	14,51%
29	Monte Grande	-70,50	-30,08	1155	83	114	180	113	37,36	117,45	26,74%
30	Vicuna	-70,70	-30,03	730	102	102	122	98	0,04	19,90	-3,63%
31	Almendral	-70,90	-29,98	430	89	99	96	98	10,52	7,56	8,79%
32	La Serena	-71,25	-29,90	15	87	90	94	89	3,79	7,92	1,99%
33	Pabellon	-70,55	-30,40	2020	157	169	194	166	7,25	23,41	5,26%
34	Las Ramadas	-70,58	-31,02	1350	325	290	345	291	-10,65	6,23	-11,78%
35	Tascadero	-70,67	-31,02	1230	287	297	345	300	3,23	20,02	4,17%
36	Hurtado	-70,68	-30,28	1200	144	132	171	133	-8,26	18,98	-8,43%
37	Tulahuen	-70,77	-30,97	1020	237	249	199	251	5,01	-15,95	5,77%
38	Cogoti 18	-70,95	-31,08	905	189	216	199	216	14,09	5,07	12,45%
39	Combarbala	-71,00	-31,17	870	226	189	347	189	-16,11	53,73	-19,66%
40	Rapel	-70,78	-30,72	870	184	193	161	194	4,39	-12,73	4,89%
41	Caren	-70,77	-30,85	740	199	206	161	208	3,44	-19,18	4,13%
42	Pichasca	-70,87	-30,38	725	132	118	131	118	-10,46	-0,79	-12,17%
43	SamoAlto	-70,93	-30,40	680	107	130	131	131	21,35	21,87	17,67%
44	Cogoti	-71,08	-31,00	650	181	187	179	187	3,22	-1,35	3,15%
45	LaPlacilla	-71,30	-30,88	400	229	167	158	167	-27,03	-30,94	-36,82%
46	Tome	-70,97	-30,82	475	167	160	161	158	-4,63	-3,87	-5,99%
47	Paloma	-71,03	-30,70	430	136	142	144	140	3,84	5,60	2,94%
48	Recoleta	-71,10	-30,50	400	108	124	131	123	14,90	21,33	12,46%
49	Pena Blanca	-71,53	-30,90	360	167	176	100	179	5,32	-40,19	6,53%
50	Sotaqui	-71,12	-30,62	280	126	114	131	113	-9,41	4,23	-11,30%
51	Punitaqui	-71,27	-30,82	410	169	187	139	187	10,44	-17,72	9,80%
52	Ovalle	-71,20	-30,60	234	109	124	131	124	13,86	20,55	12,18%
53	LaTorre	-71,37	-30,62	134	125	120	116	118	-4,24	-7,30	-6,13%
54	LosMolles	-70,58	-30,73	2640	102	289	194	280	183,37	90,07	63,51%
55	Totoral	-70,95	-27,88	150	34	36	71	37	3,56	106,33	6,35%
56	Transito	-70,27	-28,87	1200	54	85	81	86	57,23	49,38	37,08%
57	CantoAgua	-70,92	-28,15	250	36	40	61	40	8,39	67,24	9,39%
58	Domeiko	-70,90	-28,93	780	45	61	96	60	36,37	115,35	25,77%
59	Tambos	-70,20	-28,98	1385	97	91	153	91	-6,60	57,51	-6,70%
60	SanFelix	-70,47	-28,93	1100	75	75	110	76	0,02	46,73	1,19%
61	Corral	-70,47	-29,10	1900	69	93	110	91	34,51	59,90	24,48%
62	Lautaro	-70,00	-27,97	1100	42	41	117	44	-1,06	179,46	4,73%
63	PastosGrandes	-69,55	-27,10	2000	39	45	86	50	17,00	121,98	22,46%
64	Jorquera	-69,75	-27,83	1800	52	48	110	50	-8,18	112,59	-3,71%
65	Manflas	-69,98	-28,13	1410	47	45	141	47	-4,41	198,76	-0,17%
66	LasVegas	-69,67	-26,68	2115	52	29	100	43	-44,20	93,78	-18,93%

67	Elibor	-70,22	-27,72	745	30	36	73	39	22,11	147,17	23,71%
68	LosLoros	-70,10	-27,83	950	38	36	73	38	-6,14	91,59	0,02%
69	Copiapo	-70,33	-27,38	370	20	30	80	32	50,70	304,71	37,60%
70	Conay	-70,15	-28,97	1450	95	89	153	89	-6,31	60,97	-6,24%
71	SantaJuana	-70,65	-28,67	560	53	47	57	47	-11,18	7,51	-12,04%
72	Vallenar	-70,73	-28,57	373	43	52	60	53	19,22	38,39	17,68%
73	Freirina	-71,07	-28,50	150	40	44	74	44	11,03	87,25	10,57%
74	Parral	-70,23	-28,97	1300	72	89	153	90	23,78	111,78	20,04%
75	ElSalvador	-69,62	-26,32	2400	23	56	100	0	146,87	339,80	0,00%

Table 10 - Precipitation gauges

Id	Runoff_stat	Catch.	Long	Lat	Catch_Total	Alt	Q_annual	P_estim	P_Fav	P_TR	RunC	Coef_Fa	CoefTR
			DD	DD	Km <sup>2</sup>	m	m <sup>3</sup> /s	mm/y	mm/y	MM	oeef	vier	MM
2	Rio Illapel en Huintil	Choapa	-70,97	-31,57	1024	775	3,36	315	198	312	33%	68%	33%
3	Rio Illapel en El Peral	Choapa	-71,25	-31,65	2027	192	3,10	271	NaN	270	18%	NaN	18%
4	Rio Choapa en Limahuida	Choapa	-71,17	-31,73	3649	260	13,08	372	NaN	300	30%	NaN	38%
5	Rio Choapa en Puente Negro	Choapa	-71,25	-31,68	3815	200	13,03	365	NaN	297	30%	NaN	36%
6	Rio Choapa en Salamenca	Choapa	-70,93	-31,82	2191	500	8,24	418	304	334	28%	57%	36%
7	Rio Choapa en Cuncumen	Choapa	-70,58	-31,97	1115	1200	10,41	459	286	381	64%	57%	77%
8	Rio Chalinga en Potrero Maitenes	Choapa	-70,93	-31,67	573	562	1,09	333	NaN	255	18%	NaN	24%
9	Rio Chalinga en San Augustin	Choapa	-70,85	-31,72	442	850	1,02	347	NaN	251	26%	21%	27%
10	Rio Chalinga en La Palmilla	Choapa	-70,72	-31,70	242	800	1,07	388	251	297	36%	193%	47%
11	Rio la Laguna en salida embalse la Laguna	Elqui	-70,03	-30,20	558	3130	2,25	238	127	243	53%	98%	52%
12	Rio Toro antes junta Rio la Laguna	Elqui	-70,10	-29,97	473	2150	0,73	201	115	206	24%	42%	24%
13	Rio Turbio en Varillar	Elqui	-70,53	-29,95	4073	860	7,11	182	82	191	30%	67%	29%
14	Rio Turbio en Huanta	Elqui	-70,38	-29,83	2804	1195	6,11	197	NaN	216	35%	NaN	32%
15	Estero Derecho Alcoguz	Elqui	-70,50	-30,22	421	1645	1,48	221	164	296	50%	76%	37%
16	Rio Claro en Rivadavia	Elqui	-70,55	-29,98	1510	820	4,69	198	118	262	50%	104%	37%
17	Rio Claro en Monte Grande	Elqui	-70,48	-30,10	1230	1120	3,57	210	NaN	284	44%	NaN	32%
18	Rio Cochiguaz en El Penon	Elqui	-70,43	-30,12	679	1360	3,20	213	104	289	70%	130%	51%
19	Rio Elqui en Algarrobal	Elqui	-70,58	-30,00	5659	760	12,34	186	91	209	37%	91%	33%
20	Rio Elqui en Almendral	Elqui	-70,90	-29,98	6598	395	11,21	177	NaN	197	30%	NaN	27%
21	Rio Hurtado en Las Breas	Limari	-70,60	-30,38	836	1645	1,20	248	NaN	282	18%	NaN	16%
22	Rio Hurtado en San Augustin	Limari	-70,53	-30,47	670	2035	3,07	261	134	303	56%	90%	48%
23	Rio Hurtado en Agostura de Pangue	Limari	-71,00	-30,43	2141	500	3,43	192	128	197	26%	49%	26%
24	Rio Hurtado en entrada embalse Recoleta	Limari	-71,07	-30,47	2256	410	2,42	189	NaN	194	18%	NaN	17%
26	Rio Rapel en Junta	Limari	-70,87	-30,70	822	485	2,14	283	167	232	29%	65%	35%
27	Rio Tascadero en Desembocadura	Limari	-70,67	-31,02	236	1370	1,69	434	294	400	52%	87%	57%
28	Rio Grande en Las Ramadas	Limari	-70,58	-31,02	691	1380	4,87	446	277	389	50%	118%	57%
29	Rio Grande en Cuyano	Limari	-70,77	-30,92	1285	870	8,63	406	249	376	52%	67%	56%
30	Rio Grande en Puntilla San Juan	Limari	-70,92	-30,70	3511	420	11,76	326	199	279	32%	74%	38%
31	Rio Mostazal en Cuestecita	Limari	-70,62	-30,82	391	1250	1,99	383	NaN	268	42%	NaN	60%
32	Rio Mostazal en Caren	Limari	-70,77	-30,83	637	700	2,05	350	180	269	29%	72%	38%
33	Rio Guatulame en El Tome	Limari	-70,97	-30,80	2460	410	3,73	250	NaN	261	19%	NaN	18%
34	Rio Guatulame en salida embalse Cogoti	Limari	-71,08	-30,98	253	625	3,25	201	NaN	185	202%	NaN	219%
35	Rio Cogoti en Fragueta	Limari	-70,88	-31,12	495	1065	2,98	338	195	403	56%	100%	47%
36	Rio Cambarbala en Ramadillas	Limari	-70,92	-31,23	190	1430	1,02	326	227	353	52%	180%	48%
37	Rio Pama en Valle Hermoso	Limari	-70,98	-31,27	155	850	0,34	290	193	303	24%	49%	23%
38	Rio Cogoti en entrada embalse Cogoti	Limari	-71,03	-31,03	751	670	3,00	295	195	341	43%	70%	37%
39	Rio Limari en Panamericana	Limari	-71,53	-30,67	11436	165	12,73	233	NaN	218	15%	NaN	16%
40	Rio Limari en Penones Bajos	Limari	-71,23	-30,62	9360	250	2,34	250	NaN	237	3%	NaN	3%
42	Rio Transito en Agostura Pinte	Huasco	-70,25	-28,93	3040	1000	4,48	145	89	165	32%	50%	28%
43	Rio Transito antes junta Rio Carmen	Huasco	-70,48	-28,75	4100	812	4,62	134	78	148	27%	48%	24%
44	Rio Carmen en Ramadillas	Huasco	-70,48	-28,75	3034	825	3,09	150	71	152	21%	44%	21%
45	Rio Carmen en SanFelix	Huasco	-70,47	-28,93	2791	1150	2,83	155	72	159	21%	45%	20%
46	Rio Carmen en el Corral	Huasco	-70,40	-29,10	2430	2000	3,74	163	NaN	166	30%	NaN	29%
47	Rio Conay en las Lozas	Huasco	-70,10	-28,93	1721	1571	2,55	149	NaN	173	31%	NaN	27%
48	Rio Copiapo en Pastillo	Copiapo	-69,97	-28,00	7452	1300	2,74	78	22	139	15%	48%	8%
49	Rio Copiapo en Lautaro	Copiapo	-69,98	-27,97	7552	1200	1,22	77	NaN	138	7%	NaN	4%
50	Rio Copiapo en la Puerta	Copiapo	-70,12	-27,80	8339	915	2,70	75	NaN	133	14%	NaN	8%
51	Rio Copiapo en Angostura	Copiapo	-70,83	-27,32	18414	48	0,59	56	NaN	108	2%	NaN	1%
52	Rio Jorquera en Vertedero	Copiapo	-69,95	-28,05	4186	1250	0,78	75	48	132	8%	11%	4%
53	Rio Pulido en Vertedero	Copiapo	-69,93	-28,08	2037	1310	1,72	79	46	153	33%	51%	17%
54	Rio Manflas en Vertedero	Copiapo	-69,98	-28,15	1015	1550	0,71	92	46	141	24%	37%	16%
57	Rio Cuncumen antes Bocatema de Canales	Choapa	-70,60	-31,83	225	1360	1,17	443	287	314	37%	106%	52%
58	Rio Pama en entrada embalse Cogoti	Limari	-71,07	-31,08	799	680	1,41	263	192	277	21%	33%	20%

Table 11 - Runoff stations